Heliyon 10 (2024) e33303

Contents lists available at ScienceDirect

Heliyon

journal homepage: www.cell.com/heliyon

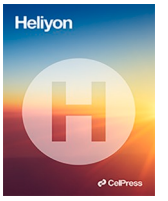

Research article

Pore-scale investigation of low-salinity water flooding in a heterogeneous-wet porous medium

Mahdi Malakoutikhah, Javad Siavashi, Jalal Fahimpour, Mohammad Sharifi *

Department of Petroleum Engineering, Amirkabir University of Technology, Tehran, Iran

ARTICLE INFO

Keywords:
Low-salinity water flooding
Wettability alteration
IFT
High salinity water flooding
Heterogenous wettability

ABSTRACT

Low-Salinity Water Flooding (LSWF) is a technique aimed at modifying the interactions between rock and fluids particularly altering wettability and reducing interfacial tension (IFT). However, there remains limited understanding of how heterogeneous wettability and the presence of Initial Water Saturation (S_{wi}) can impact the effectiveness of LSWF. This study contributes to a deeper understanding of LSWF mechanisms in the context of heterogeneous wettability, while also considering S_{wi}. The simulations were conducted using OpenFOAM, employing a non-reactive quasi-three-phase flow solver that accounts for wettability alteration and IFT reduction during the mixing of Low-Salinity (LSW) and High-Salinity Water (HSW). A heterogeneous pore geometry is designed, and four distinct scenarios are simulated, encompassing both heterogeneous and homogeneous wettability conditions while considering the presence of S_{wi}. These scenarios included secondary High-Salinity Water Flooding (HSWF), tertiary and secondary LSWF. Notably, the simulations reveal that secondary LSWF consistently yields the highest oil recovery across all scenarios, achieving recovery rates of up to 96.98 %. Furthermore, the presence of S_{wi} significantly influences the performance of LSWF in terms of oil recovery, particularly in heterogeneous wettability conditions where it boosts recovery by up to 3.5 %, but in homogeneous wettability, it decreases recovery by nearly 26 %. These simulations also underscore the pivotal role played by the distribution of oil and HSW phases in profoundly affecting the outcomes of LSWF.

1. Introduction

The ability to extract the most hydrocarbons possible from producing wells of a reservoir system is of paramount importance to the oil and gas industry [1,2]. Nearly 60 % of the world's oil reserve is contained within carbonate reservoirs, and research indicates that 70 % of this oil cannot be extracted due to the heterogeneous wettability state associated with these reservoirs [1,3–6]. Water Flooding is a prevalent method to improve oil recovery, however, this strategy, known as High-Salinity Water Flooding (HSWF), is incapable of recovering more than 30–40 % of the oil because of its inappropriate salinity and ionic content. However, multiple studies have proven that Low-Salinity Water Flooding (LSWF), which employs water with a lower salt content and corrected ions, has the potential to recover more oil than HSWF by altering the wettability to a favorable condition [7–19]. Since its first discovery in the late 1950s [20,21], LSWF has been the subject of ongoing research (beginning in 1999) as it is one of the most cost-effective and eco-friendly ways of improving oil recovery [2,3,21–24]. It is important to note that in some cases, even in field experiments, LSWF did not result in increased oil recovery. The reasons for this lack of consensus are attributed to various mechanisms, which will be explained next

* Corresponding author.
E-mail address: m_sharifi@aut.ac.ir (M. Sharifi).

https://doi.org/10.1016/j.heliyon.2024.e33303
Received 13 June 2024; Accepted 18 June 2024
Available online 21 June 2024

[25–27].

Several experimental investigations have been carried out to identify the LSWF mechanisms responsible for improved oil recovery: Fine migration was the first process hypothesized to explain low-salinity-induced oil recovery [28–30]. Some researchers found mobile fines like kaolinite improved oil recovery, while several experiments reported no additional oil recovery by LSWF under fines present, suggesting it is not the key mechanism [31–34]. The second mechanism hypothesized by Austad et al. [35], involves the desorption of organic material from clay surfaces through local pH elevation at the clay-water interface. Local pH increases induce reactivity between adsorbed basic and acidic material, as in an acid-base proton transfer, and could alter wettability to a favorable (water-wet) condition [36]. Larger et al. [34] proposed a third mechanism referred to as Multicomponent Ionic Exchange (MIE). Low-salinity brine injection desorbs positively and negatively charged organic molecules via MIE. They demonstrated that connate water with divalent ions like (Ca^{2+}) is necessary for oil recovery to occur in a tertiary injection approach. Additionally, negative ions such as sulfate play a crucial role in driving oil from the surface. In a carbonate reservoir, the cation serves to replace the positive charge on the surface. Winsauer and McCardell [37] proposed a fourth process known as double-layer expansion. By lowering the concentration of ions surrounding particles, Low Salinity Water (LSW) injected into the reservoir expands the second layer of ions, releasing oil trapped on the rock surface. According to Ligthelm et al. [38], the major mechanism of LSWF is wettability alteration toward water wetness, which develops due to double-layer expansion. Also, Nasralla and Nasr-El-Din [39]claimed that the major mechanism for LSWF to recover more oil is the expansion of the double layer, however, the molecular research conducted by Mehana and Fahes [40] rejected the double layer expansion as a process during LSWF. The fifth mechanism is wettability alterations, where LSWF affects the water layer that separates oil from the mineral surface to make the mineral more water-wet [7,41–45]. Buckley [46] postulated that osmotic pressure may be a sixth mechanism to enhance oil recovery as LSW enters the reservoir due to varying salinities. Follow-up studies legitimated this theory [47–53]. Austad [54] listed the salting effect as the seventh mechanism for LSWF, but few studies support this mechanism [35,39,55]. Additional information regarding the associated LSWF mechanism can be found in Katende and Sagala study [21]. Other researchers like Kar et al., 2022 [56] discussed oil-brine interfacial viscoelasticity and believed that viscoelasticity plays a more important role than wettability and IFT in oil recovery. Most studies confirm that LSWF induces wettability alterations [8,32,57–60], yet the primary mechanism remains ambiguous. Experimental studies are a direct way to investigate LSWF, but they only provide macroscopic parameters and do not demonstrate fluid flow behavior or phase distribution. However, thanks to technological advances and non-destructive imaging methods like micro-CT, micro-scale simulation permits detailed modeling of fluid flow behavior and phase distribution and we can now comprehend LSWF in greater depth than was previously possible [16].

As previously mentioned, technological advancements have allowed us to use micro-CT to obtain a realistic and representative pore geometry from selected porous materials. The micro-CT scan images were put through a series of image processing steps to generate the binary digital model that discriminated the pore and solid regions [12,61–65]. Pore-Scale Simulations (PSS) allow for the tracking of phase distribution and additional characteristics not achievable in experimental research by means of numerical simulations utilizing the derived digital model [61,66]. Direct Numerical Simulation (DNS) and Pore Network Modeling (PNM) are two major categories that describe different types of PSS techniques [9,17,20,61,66–69]. Two of the most well-known DNS techniques, Computational Fluid Dynamics (CFD) [70–73] and the Lattice-Boltzmann Method (LBM) [70–75], are applied directly to the digital rock model by discretizing the computational domains (meshing procedure) and solving the corresponding equations in each discrete element (mesh) [76]. DNS methods have the potential to capture transport phenomena accurately, but their high computational cost makes them impractical in specific cases [61]. As an alternative, PNM simplifies the structure of porous media to a representative pore network comprising of pore bodies and pore throats, resulting in a reduced computational cost at the expense of losing accuracy. DNS techniques are preferred to research LSWF at the pore scale because of the intricacy involved and the necessity for reliable tracking of fluid displacement and distribution pattern.

DNS methods have been widely employed by researchers to precisely capture LSWF fluid flow dynamics. The literature can be divided into two categories: studies that used DNS methods to reveal and explore LSWF mechanisms and studies that used DNS to model Interfacial Tension (IFT) and wettability variations in several porous geometries. Regarding the first category, Zaretskiy et al. (2012) [77] developed first pore scale reactive transport solver based on the finite element – finite volume approaches in a 3D sandstone digital model. Maes and Geiger (2018) [78] continued previous work and presented a novel pore-scale reactive transport solver for modeling of LSWF at pore scale by coupling OpenFOAM and PHREEQC. The presented solver was capable of modeling the effect of surface complexation on rock surface potential and wettability based on pH variations. Using the zeta potential values obtained from crude oil/water and water/carbonate in an experiment, Abu-Al-Saud et al. (2020) [79] utilized DNS for the simulation of a single oil droplet in a single pore surrounded by water to create a model that takes the electrical double-layer expansion concept into account. An et al. (2022) [80] proposed an innovative GPU-enhanced LBM that took into account the time scale of detachment in addition to the influence of buoyancy and interfacial forces (known as Bond number) on droplet detachment. Pourakaberian et al. (2022) [81] performed numerical simulations based on the coupled Poisson Nernst-Planck equations to investigate the impact of electrokinetic events in the thin brine film on wettability alteration with time in LSWF. Regarding the second category of the literature studies, Aziz et al. (2019) [57] modeled wettability alteration during LSWF using OpenFOAM but omitted the chemical reaction at the pore scale and instead assumed a linear relationship between scaled salinity and contact angle value. However, Akai et al. (2020) [82] claimed that Aziz et al. did not account for the water film penetration that occurs between oil, water, and solid contact. To investigate the impact of water film on wettability alteration, Akai et al. developed an LBM-based technique and an ion transport model to simulate LSWF using a 3D digital model of the Bentheimer sandstone. In 2021, Alizadeh et al. [8] [83,84] considered IFT variation alongside wettability alteration during LSWF to examine the flow behavior in various geometries from single pore to 2D complex pore geometries. Namaee et al. [85] investigated the impact of initial wettability, capillary number and salt dispersion in a pore doublet model on oil recovery during LSWF utilizing OpenFOAM and Volume of Fluid (VOF) model for multiphase flow simulation. According

to the literature, the majority of previous studies have concentrated on examining wettability alterations caused by LSWF, often assuming a constant homogeneous contact angle. However, there is a significant gap in research regarding how LSWF behaves as a wettability modifier in porous media under conditions of heterogeneous wettability distribution. Given that wettability plays a pivotal role in determining fluid distribution following an LSWF procedure, its significant influence on flow patterns during multiphase flow displacement cannot be overstated. Despite the fact that plenty of studies have been done on the topic, it is still unclear how the complicated wettability distribution present in real porous systems would affect LSWF behavior Furthermore, the effectiveness of LSWF has not been extensively studied in the presence of initial water saturation (S_{wi}). Notably, S_{wi} has been disregarded in all previous research endeavors.

The present investigation focuses on examining the influence of wettability on the LSWF process at the pore scale. To achieve this, a simulation methodology utilizing a modified VOF multiphase model, the OpenFoam solver, and a 2D heterogeneous pore geometry is proposed. The primary objective of this study is to compare the effects of wettability on LSWF behavior and oil recovery across various scenarios of wettability distribution. These scenarios include homogenous distributions as well as flow-based heterogeneous distributions, which aim to mirror real reservoir rock wettability conditions. Additionally, the study explores the impact of injection scenarios and considering S_{wi} on LSWF behavior. The organization of the rest of the paper is as follows. Section 2 will explain methodology, utilized geometries, mathematical modeling, and various numerical simulation scenarios. In Section 3, solver validation, mesh dependency analysis and the results of LSWF behavior in various wettability, injection scenario and initial fluid distribution conditions will be discussed. Finally, conclusions are made in section 4.

2. Methodology

The current section aims to describe the details related to the utilized workflow, revealing the effect of wettability distribution (heterogeneity) on the LSWF behavior and overall performance. The OpenFOAM package, an open-source CFD solver, is utilized to simulate two and pseudo three-phase non-reactive flow that occur in various injection scenarios during LSWF. First, to validate the numerical simulation performed by the utilized software, a pore-doublet geometry based on the Alizadeh et al. [83] study is created and discretized (meshed) by a similar procedure implemented in the mentioned study. Subsequently, the flow behavior and fluid distribution in the pore-doublet model during the HSWF and LSWF are compared to the literature studies [83,86]. To accurately examine the effect of heterogeneous wettability on the LSWF, a 2D Heterogenous pore geometry is utilized and the optimum number of elements in meshing procedure is determined through mesh dependency analysis. Subsequent to the mesh dependency analysis, two distinct wettability conditions are considered for the further simulations, a homogeneous wettability condition was defined by assuming a constant contact angle value and a heterogenous wettability distribution, based on saturation distribution at the end of drainage simulation and considering different contact angle values for the wall boundaries. Moreover, the effect of S_{wi} on the flow behavior during LSFW is also considered based on the performed drainage simulation. For all wettability conditions and initial fluid distribution patterns, different injection scenarios are considered to investigate the flow behavior of HSFW and LSWF. A summary of the utilized workflow is depicted in **Figs. S–1 (Supplementary Material)**.

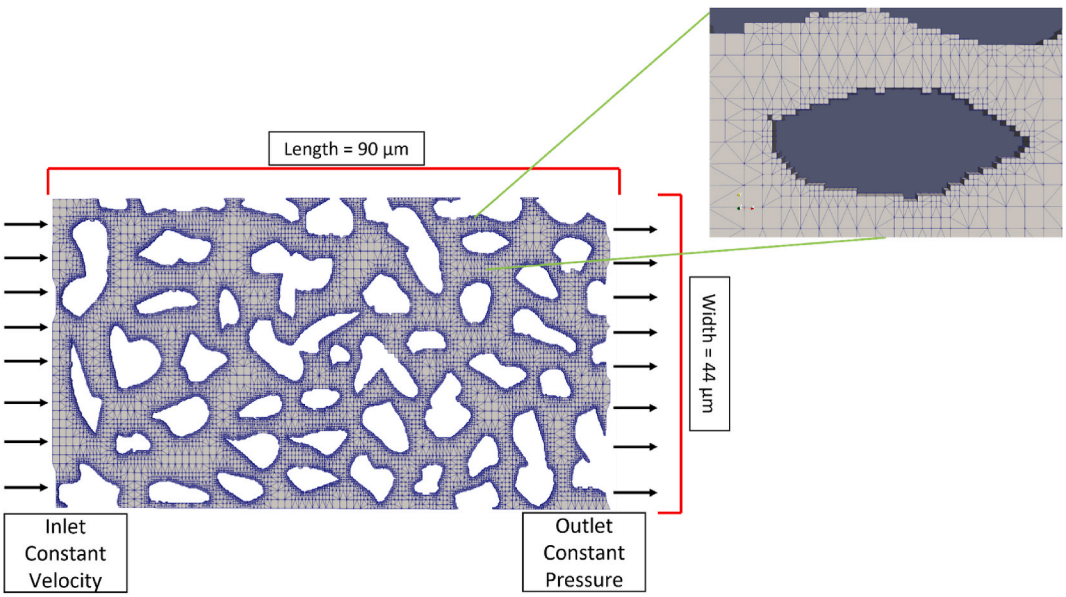

Fig. 1. 2D heterogenous geometry.

2.1. Model geometry

In this research, two separate geometries are employed: a basic pore doublet model and a 2D heterogeneous porous model. These geometries serve the purposes of validating the solver and exploring LSFW behavior on a pore-scale level. Further elaboration on each geometry can be found in the subsequent sections.

2.1.1. Pore doublet geometry

To validate the utilized solver a pore doublet geometry is designed which is illustrated in **Figs. S–2a (Supplementary Material)**. The pore doublet length and total height is about 24 μm and 17 μm respectively and contains two capillary tubes with different width of 3 μm and 7 μm for narrow and wide capillary tubes, respectively. In general, pore doublet geometry is designed in a way that could accurately represent and maintain the features of the pore doublet that has been experimentally studied by Chatzis and Dullien (1983) [86]. Such a design would allow us to validate our numerical simulation based on their experiment observation. From the left side of pore doublet, the displacing phase is injected into the pore doublet at a constant velocity. The outlet, located at right (end) facet of the pore doublet is assigned with a constant pressure condition while a no-slip condition is imposed at the wall boundaries. As shown in **Figure S-2(b, c) (Supplementary Material)**, the geometry is discretized using a meshing strategy analogous to that described by Alizadeh et al. [83]. The final mesh, resulted in grid size of 0.35 μm with tolerance of 0.05 μm, compared to the grid size of 0.4 μm reported by Alizadeh et al. [83].

2.1.2. 2D heterogenous geometry

To investigate LSWF behavior in a complex 2D porous model at various wettability, initial fluid distribution and injection conditions, a synthetic 2D Heterogenous geometry is designed with 90 μm length and 44 μm width depicted in Fig. 1. The constant velocity condition is assigned to the inlet of the geometry located at the left part of the model and the constant pressure condition is assigned to the outlet facet located at the right end of the model. The no-slip boundary condition is considered for the walls of the pore geometry.

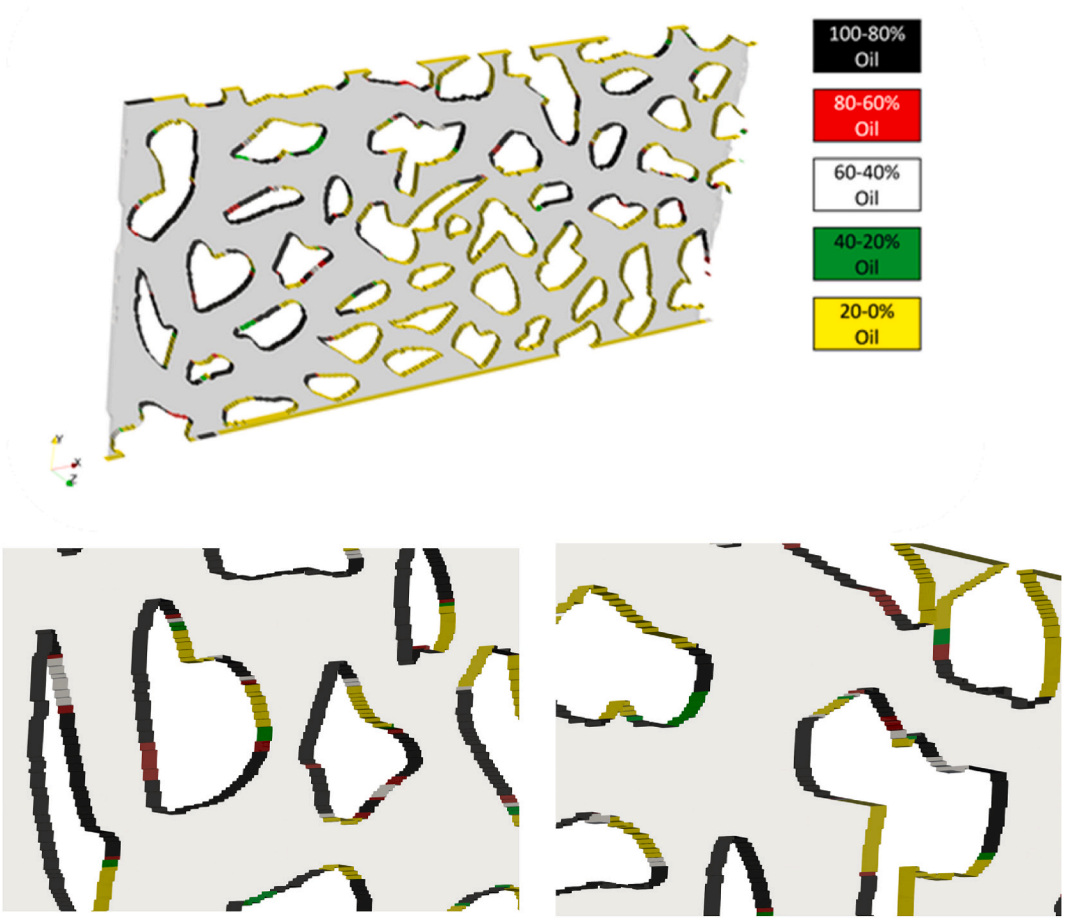

Fig. 2. A schematic of heterogeneous wettability distribution based on the oil fraction in walls faces categorized into five classes.

2.2. Mathematical modeling

In this study, OpenFOAM is employed to simulate quasi-three-phase flow. OpenFOAM provides a range of solvers suitable for multiphase flow, and for this purpose, the interFoam solver is utilized. This solver is specifically designed for modeling incompressible and immiscible two-phase flow while also tracking fluid-fluid interfaces via the VOF multiphase model. To incorporate the third fluid, represented as LSW, additional equations are introduced into the interFoam solver [15]. The volume fraction (α) represents the fluid present in each computational cell which α_1 and α_2 ($\alpha_2 = 1 - \alpha_1$) are oil and High-Salinity Water (HSW) volume fractions, respectively. The volume fraction field is determined by solving **Equation (1)**:

$$\frac{\partial \alpha_1}{\partial t} + \nabla.(\alpha_1 \boldsymbol{u}) + \nabla.(\alpha_1(1-\alpha_1)\boldsymbol{u_r}) = 0 \tag{1}$$

where u is velocity field and $u_r = u_1 - u_2$ is the relative velocity at the interface between oil and HSW. Fluid properties such as density and viscosity are calculated using a weight function expressed in **Equations 2** and **Equation 3**, respectively:

$$\mu = \mu_1\alpha_1 + (1-\alpha_2)\mu_2 \tag{2}$$

$$\rho = \rho_1\alpha_1 + (1-\alpha_2)\rho_2 \tag{3}$$

where μ_1 and ρ_1 represent the viscosity and density of oil and μ_2 and ρ_2 represent the viscosity and density of HSW. The mass continuity and momentum equations are expressed in **Equation (4)** and **Equation (5)**, respectively:

$$\nabla.\boldsymbol{u} = 0 \tag{4}$$

$$\frac{\partial \rho \boldsymbol{u}}{\partial t} + \nabla.(\rho \boldsymbol{u}\boldsymbol{u}) = -\nabla p + \left[\nabla.\left(\mu\left(\nabla \boldsymbol{u} + \nabla \boldsymbol{u}^T\right)\right)\right] + \boldsymbol{F}_{sa} \tag{5}$$

the body forces which represent by F_{sa} including interfacial forces and is expressed in **Equation (6)**:

$$\mathbf{F}_{sa} = \rho \mathbf{g}.\mathbf{n}_z + \int_\Gamma \sigma\kappa\delta(\mathrm{x}-\mathrm{x_s})\hat{\mathrm{n}}\mathrm{d}\Gamma(\mathrm{x_s}) \tag{6}$$

where the Γ is the liquid-liquid interface and $\delta(\mathrm{x}-\mathrm{x_s})$ is the Dirac delta function, κ is the interface curvature, and σ is the interfacial tension between the two fluids and $\hat{\mathrm{n}}$ is the unit vector. The interface curvature and the unit vector are expressed in **Equation (7)** and **Equation (8)**, respectively:

$$\kappa = -\nabla.\left(\frac{\nabla\alpha_1}{|\nabla\alpha_1|}\right) \tag{7}$$

$$\hat{\mathbf{n}} = \frac{\nabla\alpha_1}{|\nabla\alpha_1|} \tag{8}$$

The LSW is considered to be miscible with HSW, and the density and viscosity remain the same despite reduction of salinity. **Equation (9)** is solved to determine the LSW volume fraction (α_3):

$$\frac{\partial \alpha_3}{\partial \mathrm{t}} + \nabla.\left(\alpha_3\mathbf{u} - D_{2,3}\nabla\alpha_3\right) = 0, \mathrm{for}\Omega_{\alpha_2} \tag{9}$$

where $D_{2,3}$ is the diffusion coefficient between LSW and HSW phases. For salinity, α_3 represent the scaled salinity mass fraction. The advection and diffusion terms $\nabla.\left(\alpha_3\mathbf{u} - D_{2,3}\nabla\alpha_3\right)$ allow the LSW to diffuse into the HSW. Regarding the miscibility assumptions, the diffusion coefficient between aqueous and oil phases is assumed to be zero to prevent diffusion between mentioned phases.

To incorporate the wettability effect into the simulations, the contact angle has been used to define the vector orthogonality to the contact line interface expressed in **Equation (10)**:

$$\hat{\boldsymbol{n}} \cdot \hat{\boldsymbol{n}}_{\boldsymbol{s}} = cos\,\theta \tag{10}$$

where the $\hat{\boldsymbol{n}}$ and $\hat{\boldsymbol{n}}_{\boldsymbol{s}}$ are vector normal to fluid-fluid interface and solid wall, respectively. To induce wettability alteration, a scaled mass fraction of LSW ($\alpha_3 = 0$) and HSW ($\alpha_3 = 1$) is considered. The contact angle was assumed to be a linear function of the scaled salinity (between 0 and 1) expressed in **Equation (11)**:

$$\theta = \theta_{HS} + \frac{(\alpha_3 - \alpha_{HS}) \times (\theta_{LS} - \theta_{HS})}{(\alpha_{LS} - \alpha_{HS})} \tag{11}$$

According to mathematical expressions described above, the modified interFoam solver is able to simulate the desired quasi-three-phase flow to accurately investigate the LSWF behavior.

2.3. Simulations scenarios

The initial series of multiphase simulations involves the utilization of the devised pore doublet model. These simulations serve a dual purpose: validating the utilized solver and drawing comparisons with experimental and numerical studies documented in the existing literature. Following this, a drainage simulation is executed to replicate the preliminary migration of oil within the 2D heterogeneous geometry. The outcome of the drainage simulation, particularly the distribution of fluids, plays a pivotal role in classifying distinct wettability conditions and exploring the impact of S_{wi} on LSWF behavior. For all simulation scenarios, constant values are assumed for fluid properties and fluid-fluid interaction parameters, as detailed in Table 1.

Further details about each simulation scenarios are discussed in following sections.

2.3.1. Validation

In this case, for the purpose of validating the solver, the pore doublet geometry is assumed to resemble the one devised in the experimental study carried out by Chatzis and Dullien (1983) [86]. According to Chatzis and Dullien (1983) [86] the experiment was conducted using two distinct injection methods. Initially, the entire pore doublet geometry was saturated with oil. Subsequently, the invading fluid (water) was injected as the non-wetting phase. In the second approach, the invading fluid (water) was introduced as the wetting phase within the pore doublet. Similarly, in line with the experiment, the initial step involved injecting water as the invading non-wetting phase into the pore doublet, displacing the oil towards the outlet. Next, the invading fluid (water) is introduced as the wetting phase to displace the oil.

Finally, in order to verify the effectiveness of the solver in simulating LSW injection, the simulation is extended until a steady-state condition is reached after injecting water as the non-wetting phase. Subsequently, LSW is introduced into the pore doublet along with the presence of oil and HSW phases.

2.3.2. Initial condition

For certain LSWF simulations, the requirement is to establish two initial parameters, namely heterogeneous wettability distribution and S_{wi}. To achieve this, the 2D heterogenous geometry is initially completely saturated with water. Subsequently, oil is introduced into the geometry as the invading fluid and the non-wetting phase, mimicking the initial migration of oil into a reservoir rock. In real-case reservoir conditions, when oil or another invading phase penetrates the porous medium, it eventually reaches a steady state, and a final equilibrium dictating the fluid configuration is established. The portion of the rock surface that come into close contact with the oil may undergo wettability alterations due to exposure to certain chemical components of the oil, changing from water-wet to oil-wet conditions. The simulation is then conducted until a steady-state condition is attained, resulting in the final fluid distribution shown in **Figs. S–3 (Supplementary Material)**. Upon migrating the oil into the water-wet reservoir rock, it became evident that the oil phase could not displace all the water after reaching a steady state. Consequently, a coexistence of oil and water within the geometry persisted. This state could serve as the initial condition for subsequent simulations and to obtain a heterogenous wettability distribution. In other words, the residual water from this simulation could act as the S_{wi} for subsequent simulations, as depicted in Figs. S–3 (Supplementary Material).

2.3.3. Heterogeneous wettability

In order to achieve the condition of heterogeneous wettability distribution, the oil that had migrated into the water-wet environment came into contact with certain parts of the wall boundaries. In the VOF method, walls are simulated using representative faces capable of containing fractions of oil and other phases ranging from 0.0 to 1.0 To introduce heterogeneous wettability, five categories of wall faces were identified based on the oil fraction values. Subsequently, contact angles for oil, HSW, and LSW are assigned to these categories, as depicted in Fig. 2 and detailed in Table 2.

In this case the heterogeneous wettability distribution is considered as the initial wetting condition of the wall boundaries and the geometry is saturated with oil, then three injection scenarios are simulated including Secondary HSWF, Tertiary LSWF and Secondary LSWF to calculate the oil recovery and observe displacement patterns.

2.3.4. Homogeneous wettability

In this scenario, the initial step involves saturating the entire 2D Heterogenous geometry with oil ($S_o = 1$), while configuring the wettability of all walls to be oil-wet ($\theta_o = 50$). Subsequently, three sequential simulations are conducted. Firstly, HSW is injected into the geometry as the invading phase, serving as a secondary HSWF to recover oil from the geometry. Once the steady state is attained with the Secondary HSWF, a tertiary LSWF is initiated, further impacting oil recovery. Lastly, in order to compare the effects of tertiary

Table 1
Fluid properties and fluid-fluid interaction parameters utilized in all simulation scenarios.

Parameters	Values	Parameters	values
HSW Density	1050 kg m^{-3}	**HSW and LSW Diffusion Coefficient**	1.0e-9 $m^2.s^{-1}$
LSW Density	1000 kg m^{-3}	**Water and oil Phase Diffusion Coefficient**	0.0 m^2 s^{-1}
Oil Phase Density	800 kg m^{-3}	**HSW and LSW Brine Scaled Concentration**	0.0–1.0
Water Phase Viscosity	0.001 Pa s	**HSW and Oil Interfacial Tension**	0.02 N m^{-1}
Oil Phase Viscosity	0.005 Pa s	**LSW and Oil Interfacial Tension**	0.005 N m^{-1}

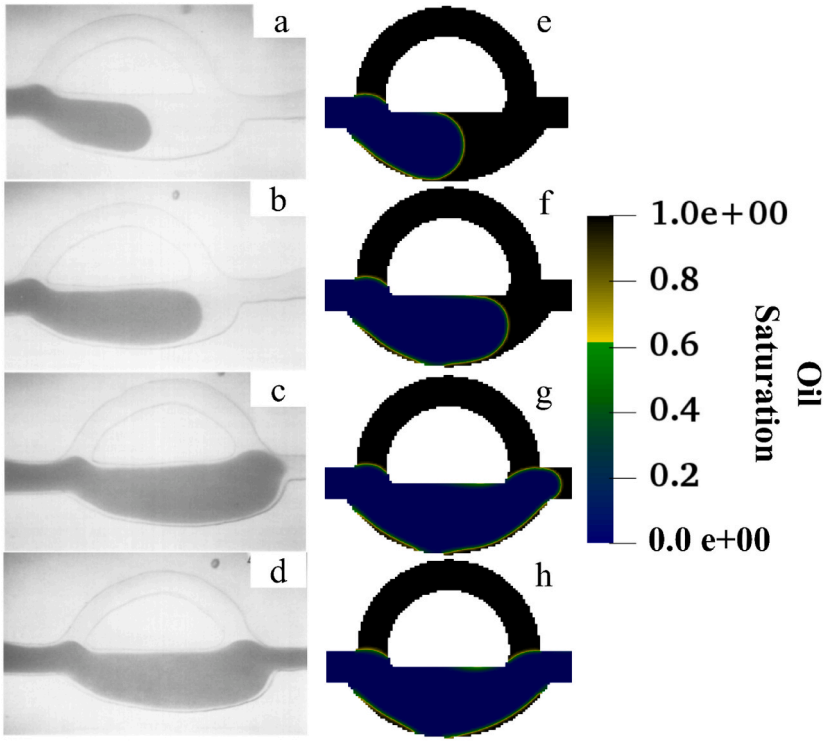

Fig. 3. Comparing the non-wet injection into the pore doublet between (a, b, c and d) experiment study by Chatzis and Dullien (1983) [86] and (e, f, g and h) performed simulations.

Table 2
Contact angle values considered for various wettability classes.

Classes	HSW contact angle (degrees)	LSW contact angle (degrees)	Oil contact angle (degrees)
100–80 % Oil	130	85	50
80–60 % Oil	110	75	70
60–40 % Oil	90	65	90
40–20 % Oil	70	55	110
20–0% Oil	50	45	130

and secondary LSWF, the entire geometry is reset to being fully saturated with oil (So = 1), and LSWF is introduced as a secondary phase.

2.3.5. Considering initial water saturation

Traditionally, all micro-scale simulations are begun with full saturation of a single phase (either oil or water). However, this study also aims to examine the impact of S_{wi} on the LSWF behavior. As oil migrates into the reservoir rock, it is unable to displace all the water present, leaving behind water in the reservoir known as S_{wi} or connate water. Commencing simulations from the final state of the drainage simulation, where both water and oil coexist within the geometry, enables the incorporation of S_{wi} considerations. The simulations encompass both homogeneous and heterogeneous wettability distribution scenarios. Additionally, three injection scenarios are investigated: secondary HSWF, tertiary LSWF, and secondary LSWF.

3. Results and discussion

This section will address the outcomes of the aforementioned scenarios. Initially, we delve into the accuracy of the solver and the influence of LSWF within the pore doublet, aiming to validate the solver and comprehend the potential impacts of LSWF on Enhanced Oil Recovery (EOR). Subsequently, we will elucidate the analysis of mesh sensitivity performed on the 2D heterogenous geometry. Lastly, an investigation of all simulation scenarios conducted for the 2D heterogenous geometry will be presented, along with an examination of the impact of LSWF on each scenario.

3.1. Pore-doublet simulation

To validate the solver, the initial step involves saturating the geometry with oil. Subsequently, water (depicted in blue) is introduced into the geometry as both the wetting and non-wetting phases. The inlet condition is defined as a constant velocity with a magnitude of 0.001 m s^{-1}, while the outlet maintains a constant pressure at 0 Pa. The walls are assigned a no-slip condition (v = 0 m s^{-1}). A contact angle of 20° is assigned to the wet phase, while the non-wetting phase contact angle is set at 160°.

As depicted in Fig. 3, the injection of non-wet water initiates from the wider region, while the oil (depicted in black) resides within a narrower section. Additionally, a portion of the oil adheres to the wall of the wider channel, resembling a thin layer of the wetting phase which is evident in Fig. 3(d–h). Ultimately, A remarkable resemblance in flow behavior between the simulations and the conducted experiments is evident in case of non-wetting injection.

In the case of wetting injection, the water moves through the narrow channel initially, benefitting from favorable capillary effects, without causing significant displacement of oil within the wider channel. As the water, functioning as the wetting phase, approaches the outlet area, the displacement of oil from the wider channel begins, eventually reaching a stable state. The fluid flow behavior observed during the simulation, illustrated in Fig. 4, aligns with the experimental findings reported by Chatzis and Dullien [86].

To explore LSWF within the pore doublet, following the injection of HSW as the non-wetting phase (which only occupies the larger channel as a result of non-favorable capillary forces), the subsequent injection of LSW (depicted in red) is observed. The outcomes of this sequence reveal a shift in wettability from non-wetting to wet conditions, resulting in the displacement of fluid within the narrow channel as illustrated in **Figs. S–4 (Supplementary Material)**.

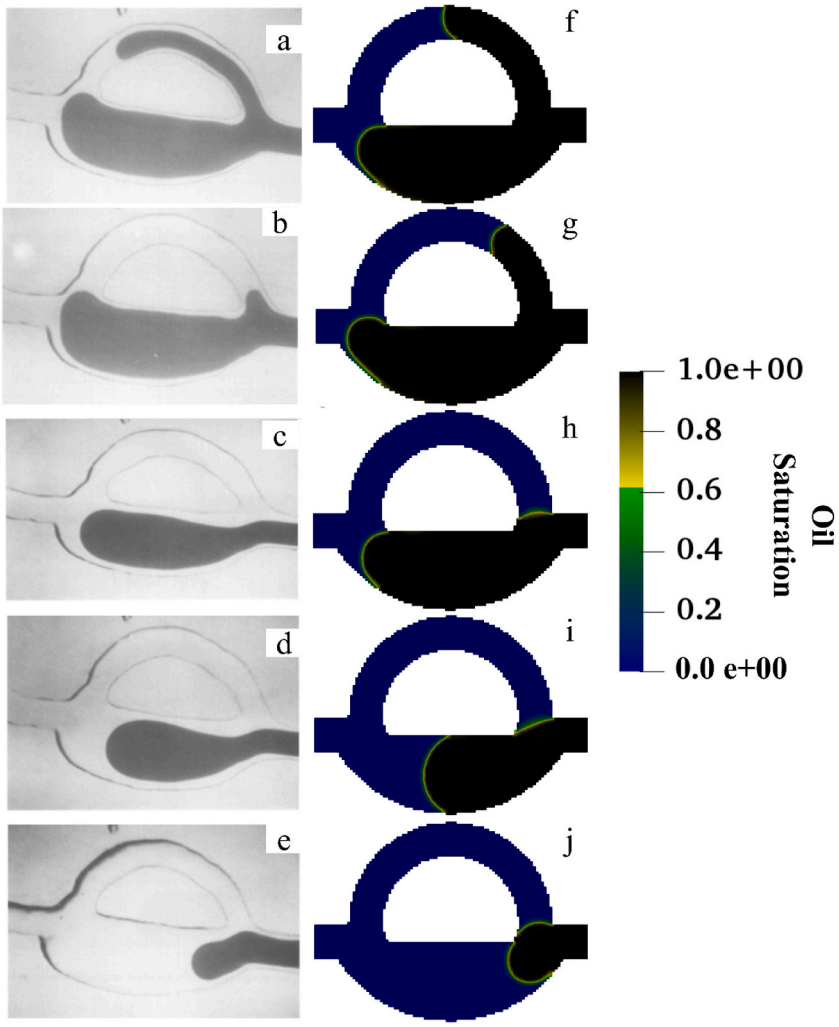

Fig. 4. Comparing the wetting injection into the pore doublet between (a–e) experiment study by Chatzis and Dullien (1983) [86] and (f–j) performed simulations.

3.2. Mesh sensitivity analysis on 2D heterogenous geometry

In order to establish an optimal mesh size for the 2D heterogeneous geometry, a comprehensive mesh dependency analysis is carried out. Determining the optimum mesh size is crucial due to its significant impact on both simulation runtime (computational efficiency) and result accuracy. To conduct this analysis, five sets of simulations are performed, involving the injection of non-wetting water into the oil-saturated geometry. The boundary conditions mirror those detailed in 3.3.2 section. Considering parameters like simulation runtime and the ultimate recovery factor as decisive factors for determining the optimal mesh size, an unstructured mesh composed of 20,456 grids, with grid volumes ranging from 2.14e-20 m^3 to 1.37e-18 m^3, is selected as the optimum mesh for subsequent simulations. The mesh dependency analysis results are presented in Table 3.

3.3. Determining initial condition through primary drainage simulation

To achieve a heterogeneous distribution of wettability (contact angles) across the wall boundaries and to establish an initial condition that accounts for the S_{wi} in various scenarios, a primary drainage simulation is conducted. The inlet boundary condition maintained a constant velocity of 0.001 m s^{-1}, while the outlet is set to a constant atmospheric pressure of 0 Pa. The wall boundary condition was defined as a no-slip condition ($v = 0$ m s^{-1}). Following this, oil is injected into the water-saturated geometry as the non-wetting phase, replicating the primary migration of the oil. The simulation is prolonged until it reaches a stable state. Fig. 5 visually illustrates the progression of oil migration into the 2D heterogeneous geometry saturated with water. This simulation reached a steady-state condition after 0.07 s.

3.4. LSWF scenarios

In this section, the LSWF behavior in the 2D heterogeneous geometry will be examined and presented. In all of these simulations, the inlet condition is fixed at a constant velocity of 0.001 m s^{-1}, while the outlet maintains a constant pressure of 0 Pa. The walls are set to a no-slip condition ($v = 0$ m s^{-1}), and the fluid properties adhere to those outlined in Table 1. According to the defined boundary conditions, the capillary number is approximately 1E-3. At this level, the simulation results are not entirely dominated by capillary forces, indicating that capillary regimes do not predominantly influence the outcomes. Based on the core-flooding protocols and simulation studies reported in the literature, we have incorporated various injection scenarios into our study. For all scenarios, HSW is injected into the model as a secondary recovery approach, while LSW is injected using both tertiary and secondary injection concepts. In the tertiary method, LSW is injected after the injection of HSW has reached a steady-state condition, at which point the oil recovery remains constant. In the secondary LSWF method, LSW is directly injected into the model as the second phase without considering any previous (HSW) injection scenarios.

3.4.1. Homogeneous wettability

In this scenario, a uniform contact angle value is allocated to all wall boundaries pertaining to a specific phase. For instance, a contact angle of 50° is uniformly assigned with respect to the oil phase across all wall boundary patches to simulate an oil-wet condition. Initially, HSW is introduced into the domain as a secondary HSWF recovery scenario, leading to an ultimate recovery value of 47.11 % original oil in place (OOIP). The evolution of fluid distribution at various time intervals is illustrated in Fig. 6.

Upon reaching a steady state condition for the Secondary HSWF, the tertiary LSWF is initiated. During this stage, the LSW mixes with the HSW, causing a reduction in contact angle with respect to the injected phase and resulting in a shift towards increased water-wet condition. This decrease in wettability follows a linear relationship with the concentration of HSW and LSW, declining from 130° (for $\alpha_{HSW} = 1$) to 45° (for $\alpha_{LSW} = 1$). The outcomes of the tertiary LSWF are presented in Fig. 7. As depicted in Fig. 7, the initial phase involves the dissolution of LSW into the HSW, leading to a reduction in IFT and contact angle. However, this reduction does not lead to immediate displacement of the oil; instead, it needs to reach a particular threshold, as indicated in Fig. 7(c), to effectively push the oil towards the outlet. Upon implementing Tertiary LSWF, the oil recovery rate increases to 82.93 % of OOIP, achieving an additional recovery of 35.82 %.

In order to draw a comparison between secondary and tertiary LSWF, the secondary LSWF scenario is simulated anew, commencing by saturating the entire geometry with oil ($S_o = 1$). The contact angles for oil and LSW are set at 60 and 45°, respectively. The boundary conditions are configured in a manner analogous to the conditions applied in the secondary HSWF. The recovery of oil from the secondary LSWF under homogeneous wettability amounted to 96.98 % of the OOIP and the evolving fluid distribution is illustrated in Fig. 8.

Table 3
Mesh sensitivity for 2D Heterogenous Geometry; according to results, third case has the optimum computational costs.

Case number	Number of grids	Recovery Factor (percent)	Simulation runtime (hr)	Related error to the fine mesh (percent)
1	8065	46.35 %	1.86	2.42 %
2	16935	46.96 %	2.65	1.14 %
3	20546	47.11 %	3.02	0.82 %
4	35896	47.39 %	5.6	0.23 %
5	61239	47.50 %	7.3	base case

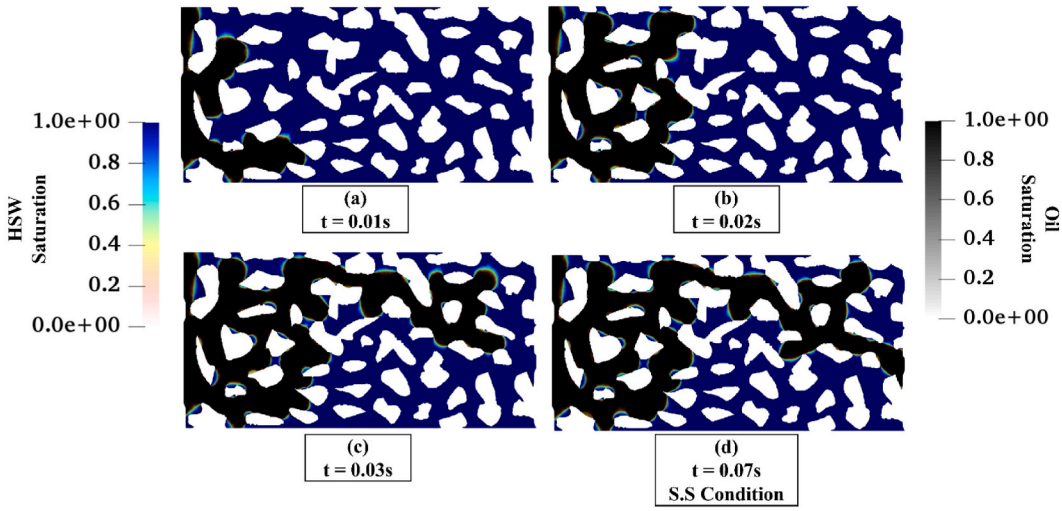

Fig. 5. Initial condition simulation involving primary oil migration to the water-wet geometry.

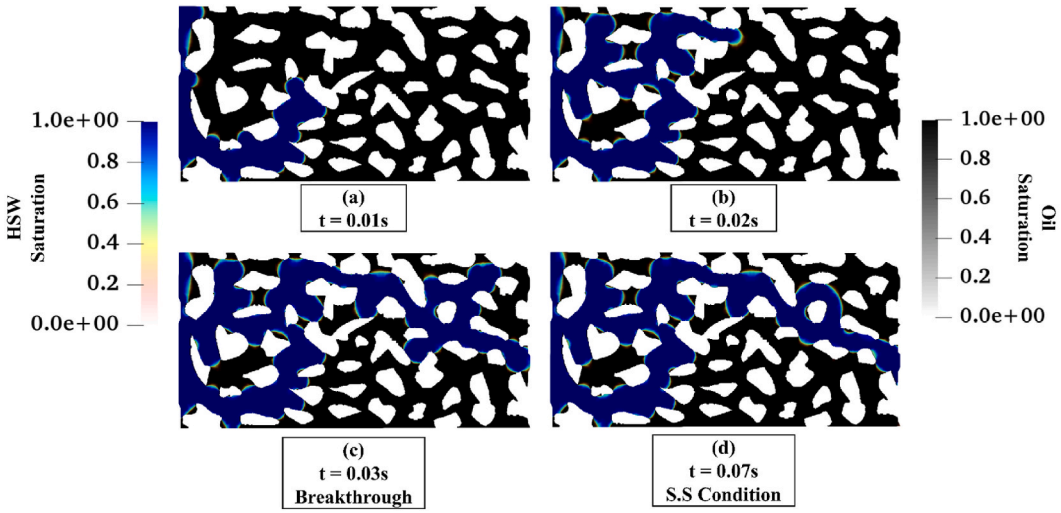

Fig. 6. Secondary HSWF in homogenous wettability condition of 2D heterogenous geometry; Blue signifies HSW, while black represents oil.

Secondary HSWF, Tertiary LSWF, and Secondary LSWF simulations collectively indicate that introducing LSW as a tertiary phase allows it to pass through the HSW phase, possibly leaving behind some remaining oil in the geometry. Although, over time, as the HSW gets diluted and transforms into LSW, some of the residual oil is swept away. However, employing LSW as a secondary phase injection seems to exhibit a more efficient sweeping effect, resulting in higher oil recovery in a shorter period of time. A comparison of the recovery curves for these simulations can be observed in **Figs. S–5 (Supplementary Material)**.

3.4.2. Heterogenous wettability

In alignment with the details provided in Section 2.3.3, the contact angles for the wall boundaries in these simulations are determined as per the specifications outlined in Fig. 2 and Table 2. Initially, the entire geometry is saturated with oil (So = 1), followed by the injection of HSW as a secondary phase from the inlet. The injection persisted until a steady-state condition was achieved, as depicted in Fig. 9. The total recovery achieved through secondary HSWF amounts to 65.36 % of OOIP, with a breakthrough time of 0.027 s. Notably, the recovery rate observed in comparison to the case of homogeneous wettability exhibited an increase of 18.25 %, while the breakthrough time saw a reduction of 0.003 s.

Following the attainment of a steady state condition through secondary HSWF, the initiation of tertiary LSWF is depicted in Fig. 10. In this scenario, the continuous phase of HSW persists from the inlet to the outlet, creating a more favorable pathway for LSW due to wettability considerations. However, as LSW traverses through the existing HSW phase, it does not yield a substantial enhancement in oil displacement. This can be attributed to the continuous presence of HSW and the pathway it offers. Consequently, the oil recovery resulting from tertiary LSWF exhibited a marginal improvement, increasing by only 1.45 % and ultimately reaching a recovery rate of

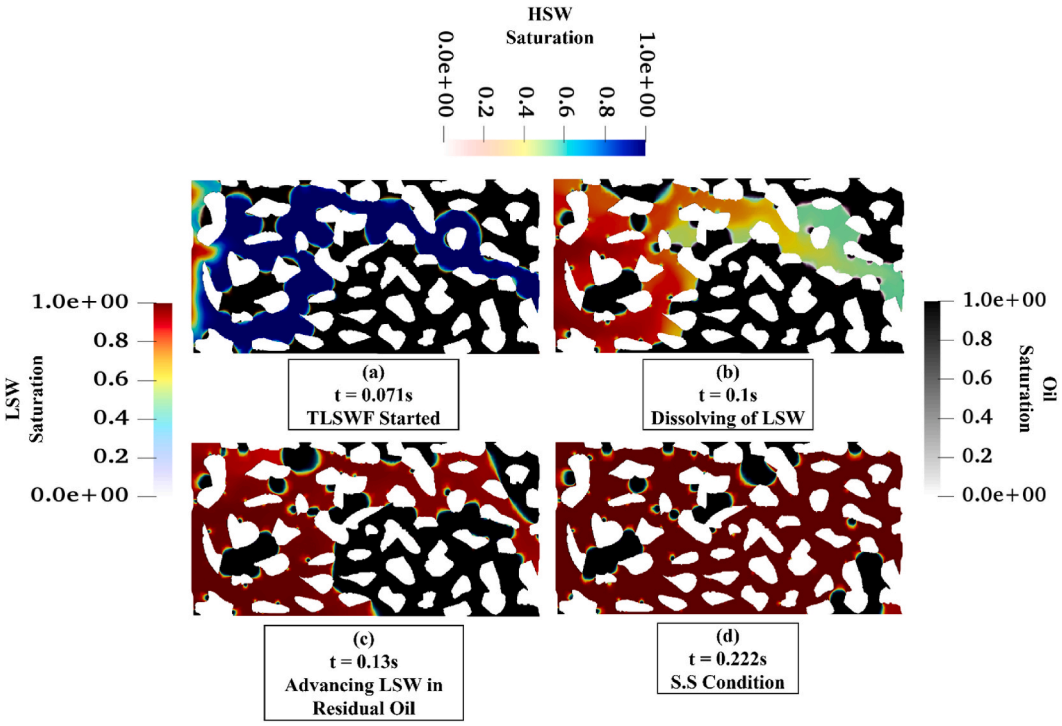

Fig. 7. Starting LSWF as a tertiary Injection recovery method into the geometry; Introducing LSW to HSW environment (a and b); Advancing into the geometry and swiping the oil toward the outlet (c); S.S condition of tertiary LSWF (d).

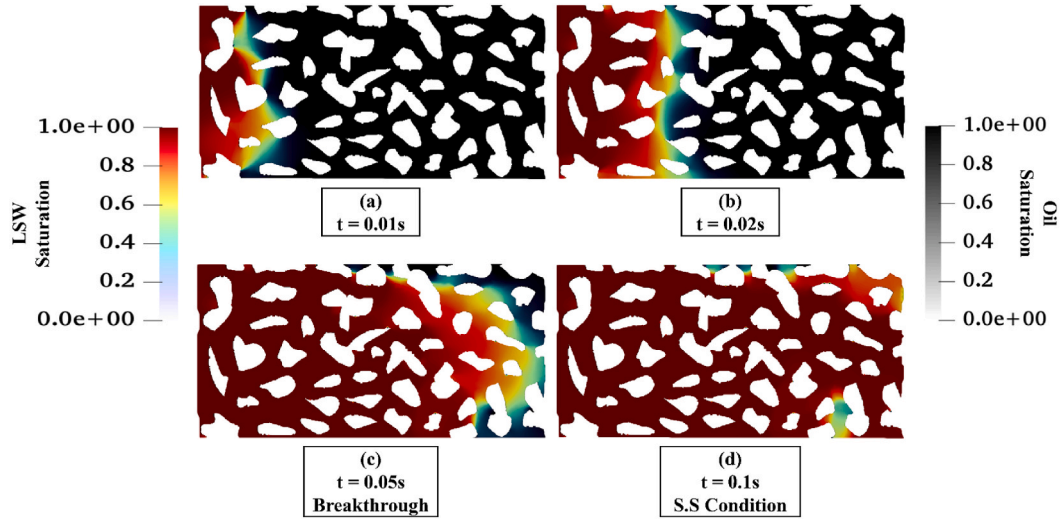

Fig. 8. Secondary LSWF at homogenous wettability condition; Dark red signifies LSW, while black represents oil.

66.81 % of OOIP.

For the purpose of comparing secondary and tertiary LSWF within the heterogeneous wettability context, the entire geometry is once again saturated with oil (So = 1), and LSW is injected into the geometry as a secondary phase, as indicated in Fig. 11. In this scenario, the oil recovery reached 92.72 % of the OOIP. However, when contrasting the impact of heterogeneous wettability against homogeneous wettability, it becomes evident that the LSW front takes on a more piston-like shape in homogeneous wettability. This distinction arises due to the fact that in heterogeneous wettability, the wettability for LSW is more favorable in the lower section of the geometry, as evidenced in Fig. 2. Consequently, LSW tends to accumulate there, resulting in a breakthrough time occurring approximately 0.003 s earlier. The oil recovery for secondary HSWF, tertiary LSWF, and secondary LSWF under heterogeneous

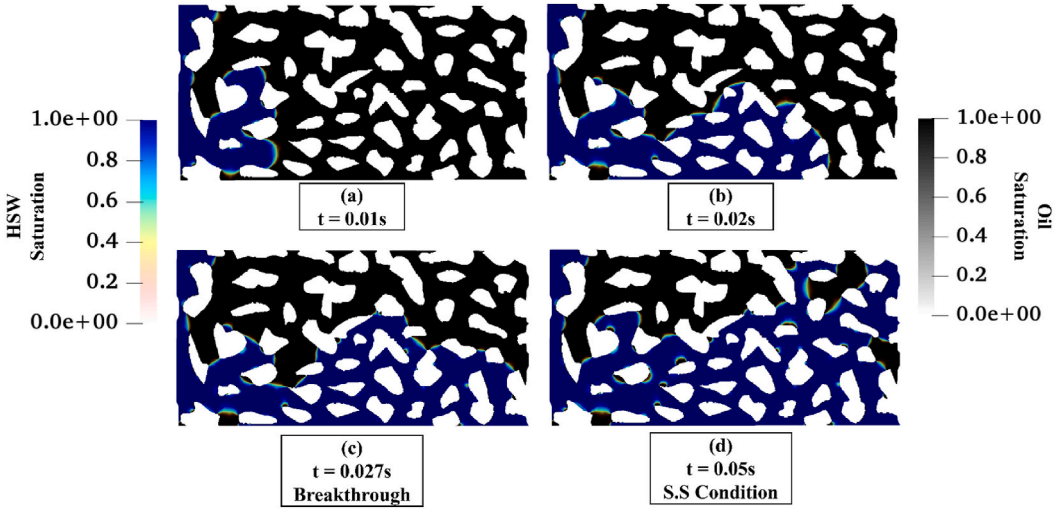

Fig. 9. Secondary HSWF in heterogenous wettability distribution, fluid distributions at breakthrough time (c); S.S condition (d).

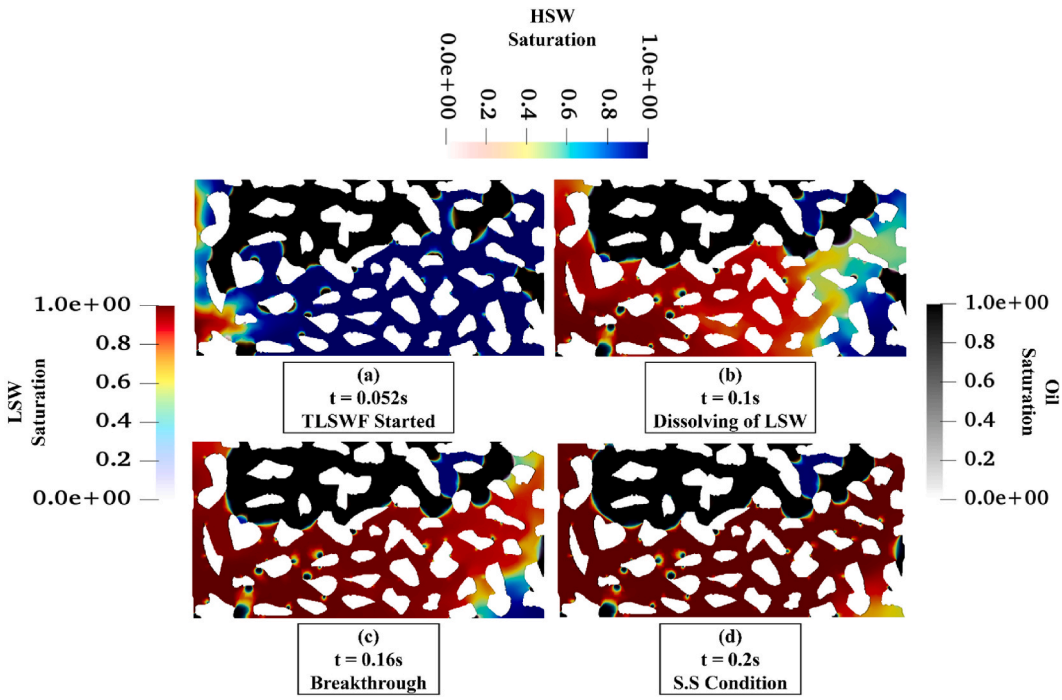

Fig. 10. Injecting LSW as a tertiary recovery method in the heterogenous wettability condition case; by dissolving LSW in HSW, the LSW reached to the outlet (c) and until reaching a S.S condition (d) there is no significant additional oil recovery.

wettability conditions is presented in Figs. S–6 (Supplementary Material).

3.4.3. Considering initial water saturation

In these simulations, following the guidelines outlined in Section 2.3.2, all simulations were replicated for both homogeneous and heterogeneous wettability conditions while also considering the presence of S_{wi}. The boundary conditions for these simulations remained consistent with those employed in the preceding simulations.

3.4.3.1. Homogenous wettability. In this specific scenario, the wettability of all walls is adjusted to an oil-wet state ($\theta_o = 50°$). Initially, the HSW is introduced into the geometry as a secondary injection scenario, as depicted in Fig. 12. Through the implementation of secondary HSWF, a total recovery of 59.24 % of OOIP is achieved.

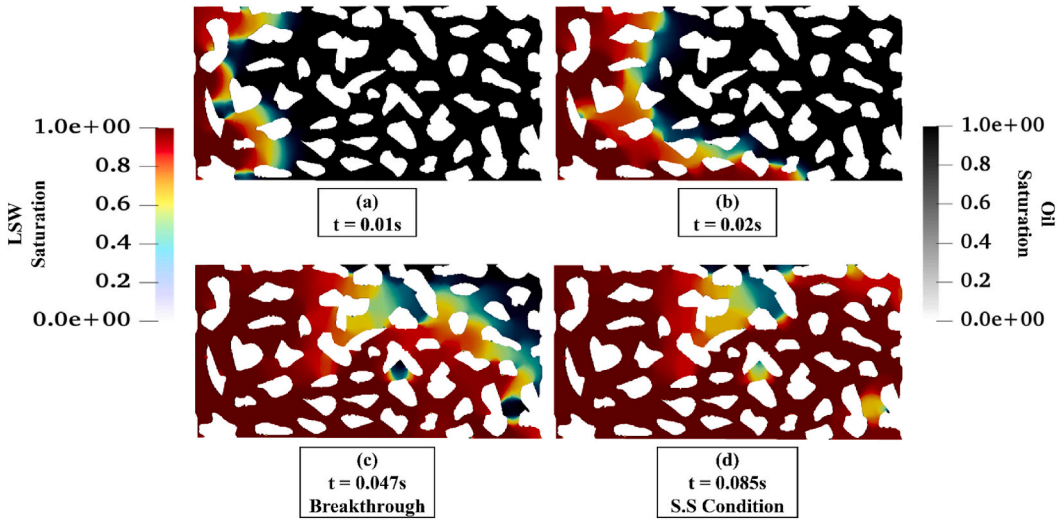

Fig. 11. Secondary LSWF in heterogenous wettability condition case; Breakthrough time (c); S.S condition (d).

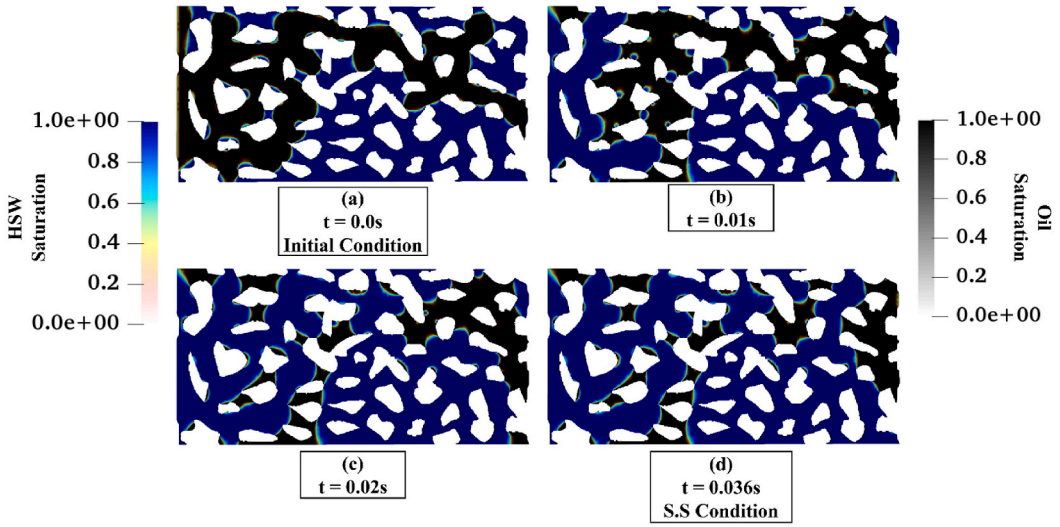

Fig. 12. Secondary injection of the HSW under homogenous wettability condition and with the presence of S_{wi}; Initial Condition (a); S.S Condition (d).

Following the attainment of a steady-state condition in the secondary HSWF, the initiation of the tertiary LSWF occurs, as shown in Fig. 13. As depicted in Fig. 13, the LSW blends with the HSW and progresses towards the outlet. However, this blending does not lead to a substantial increase in oil recovery, resulting in an oil recovery rate of 62.44 % of OOIP with an additional recovery of 3.2 %.

For the purpose of comparing secondary and tertiary LSWF, the water and oil saturation levels were returned to their initial conditions in the presence of irreducible water saturation (S_{wi}), and the initiation of secondary LSWF ensued, as depicted in Fig. 14. Additionally, as there is an S_{wi} within the geometry, the recovery achieved through secondary LSWF reached approximately 70.78 % of the OOIP. This outcome can be attributed to the fact that, the presence of S_{wi} decreases the final oil recovery due to providing more continuous preferential pathways to LSW. Consequently, the effect of secondary LSWF on producing significant additional oil recovery is diminished.

However, when LSWF is introduced as a secondary phase, the continuous nature of the oil phase facilitates a more pronounced impact from LSWF, leading to enhanced oil recovery. For a comprehensive comparison between secondary HSWF, tertiary LSWF, and secondary LSWF, please refer to **Figs. S–7 (Supplementary Material).**

3.4.3.2. Heterogenous wettability. In this particular scenario, the geometry is characterized by heterogeneous wettability condition and presence of S_{wi}, as specified in Sections 2.3.3 and 2.3.5. The initial contact angles for the wall boundaries are assigned based on the guidelines outlined in Section 2.3.3 while also accounting for the presence of irreducible water saturation as detailed in Section 2.3.5.

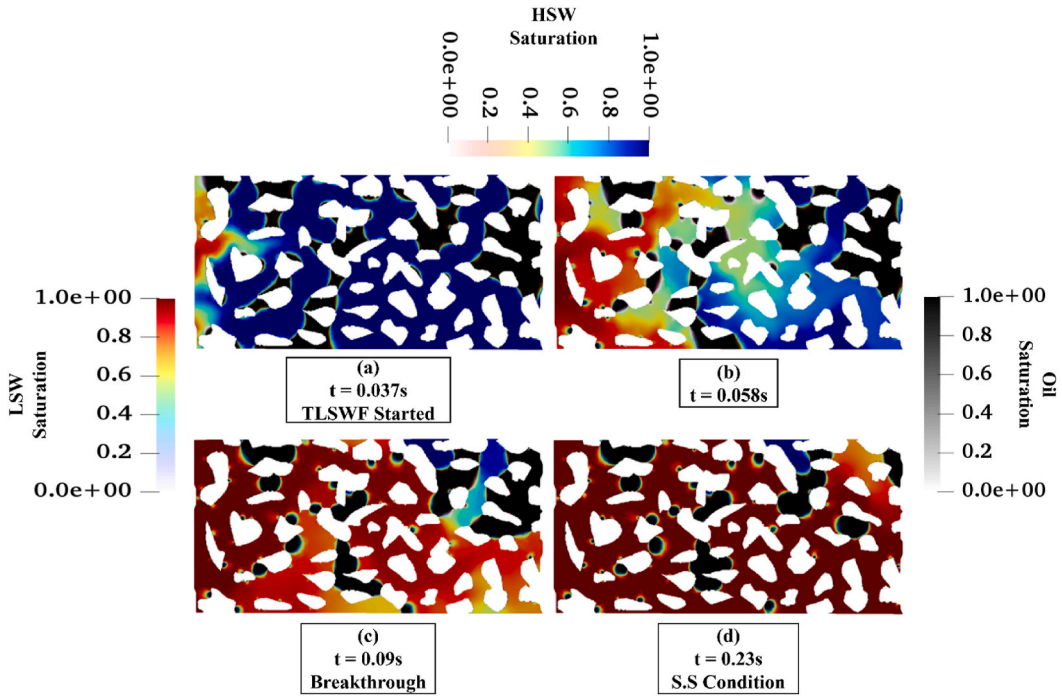

Fig. 13. Tertiary injection of the LSW under homogenous wettability condition with the presence of S_{wi}; Starting of LSWF (a); Breakthrough (c); S.S Condition (d).

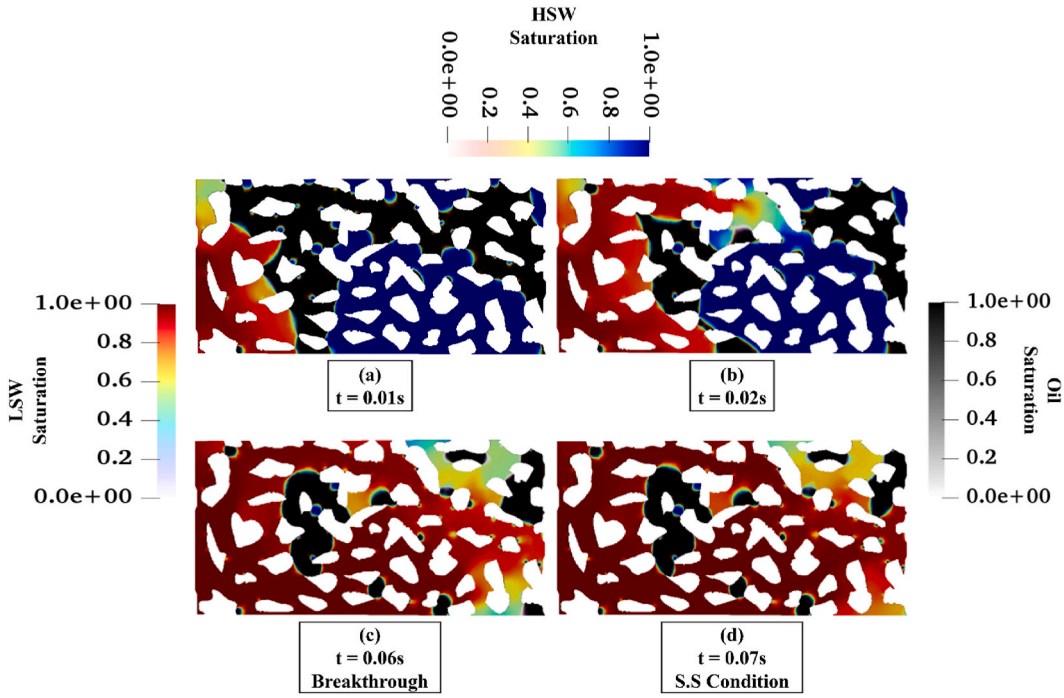

Fig. 14. Secondary injection of the LSW under homogenous wettability condition with presence of S_{wi}; Breakthrough Time (c); S.S Condition (d).

The initiation of HSWF as a secondary phase is depicted in Fig. 15. Through this approach, a substantial oil recovery of 49.28 % of OOIP is accomplished.

Upon the attainment of a steady-state condition through secondary HSWF, the commencement of tertiary LSWF is illustrated in

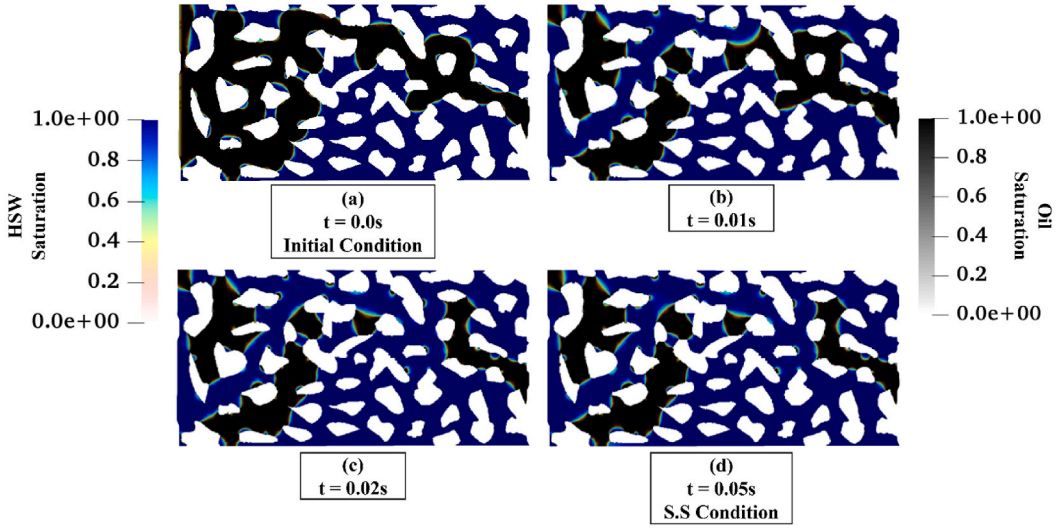

Fig. 15. Secondary injection of the HSW under heterogenous wettability and with the S_{wi} presence; Initial condition (a); S.S condition (d).

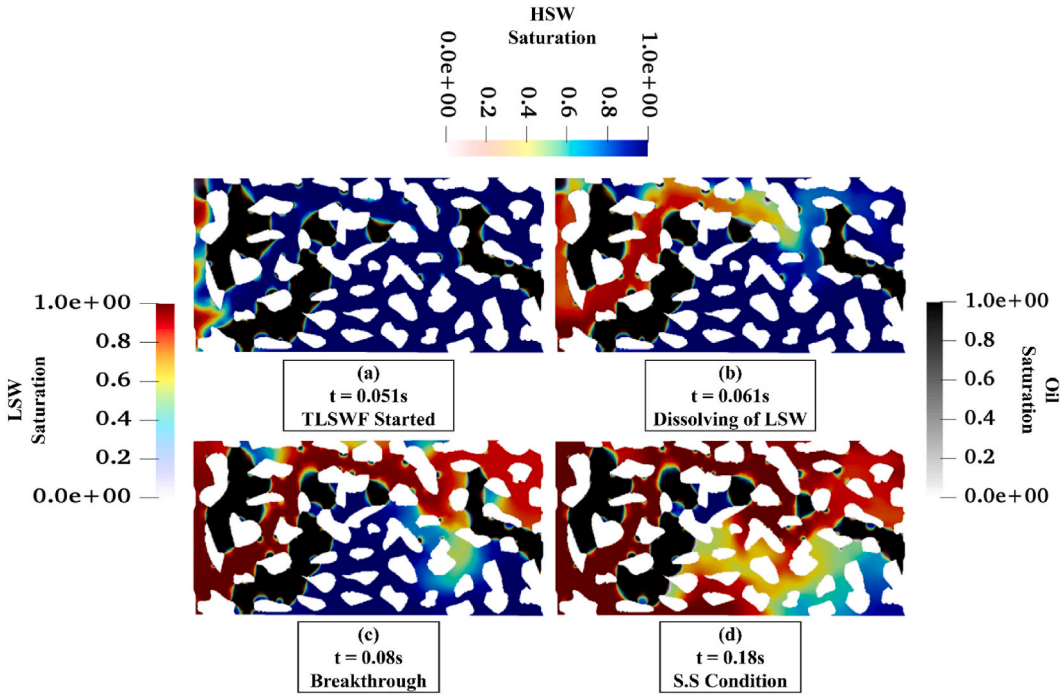

Fig. 16. Tertiary injection of the LSW under heterogenous wettability condition and with the S_{wi} Presence; Breakthrough time (c); S.S condition (d).

Fig. 16. The application of tertiary LSWF in a heterogeneous wettability setting yields an oil recovery of 55.45 % of the OOIP, resulting in an additional oil recovery of 6.17 % of the OOIP.

In order to draw a comprehensive comparison between secondary and tertiary LSWF scenarios within the context of heterogeneous wettability conditions, taking into account the presence of S_{wi}, the initial saturation levels of both water and oil were returned to their original state. Subsequently, the initiation of secondary LSWF is illustrated in Fig. 17. Notably, in the case of secondary LSWF, a substantial oil recovery rate of 73.77 % of the OOIP is achieved. This pronounced enhancement in oil recovery through secondary LSWF underscores its potential efficacy in promoting oil displacement within reservoir systems characterized by heterogeneous wettability conditions and considering the presence of irreducible water saturation. For a more in-depth comparative analysis, please refer to **Figs. S–8 (Supplementary Material).** In this series of simulations, the interplay between heterogeneous wettability and S_{wi} presence brings forth varying degrees of oil recovery, showcasing the influence of these factors on enhanced oil recovery. The

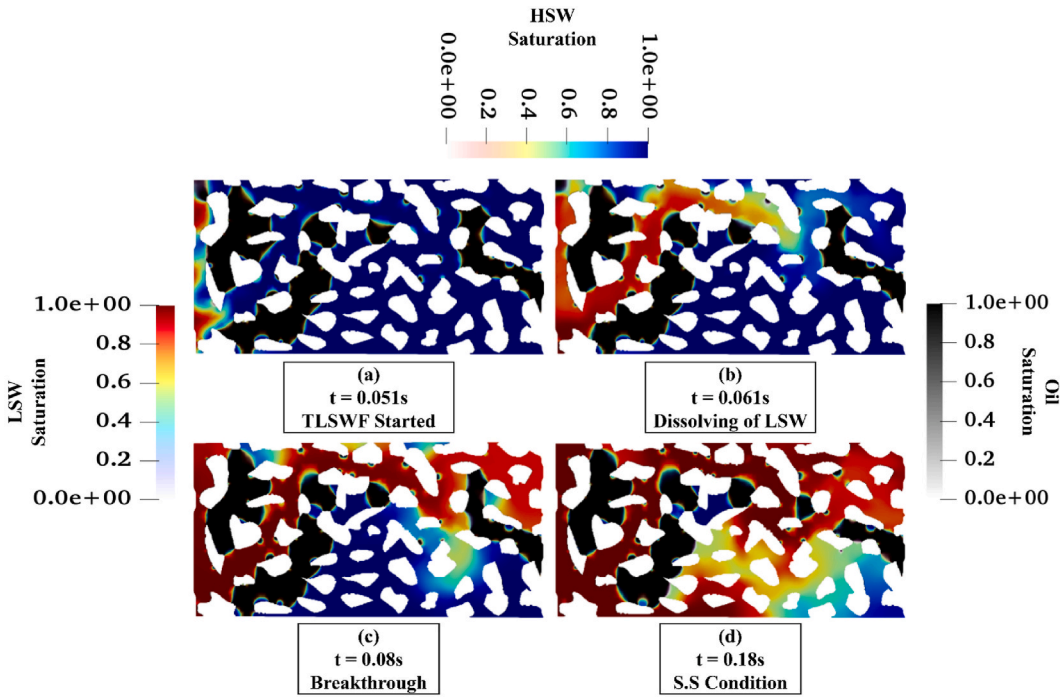

Fig. 17. Secondary injection of the LSW under heterogenous wettability and with the S_{wi} presence; Breakthrough time (c); S.S condition (d).

outcomes demonstrate the potential of employing such strategies to optimize oil recovery mechanisms in reservoir simulation scenarios.

3.5. *Evaluation of all injection scenarios*

In this section, secondary HSWF, Tertiary LSWF and Secondary LSWF in all scenarios will be compared and the efficiency of HSWF and LSWF in homogenous and heterogenous wettability condition in presence of S_{wi} will be discussed.

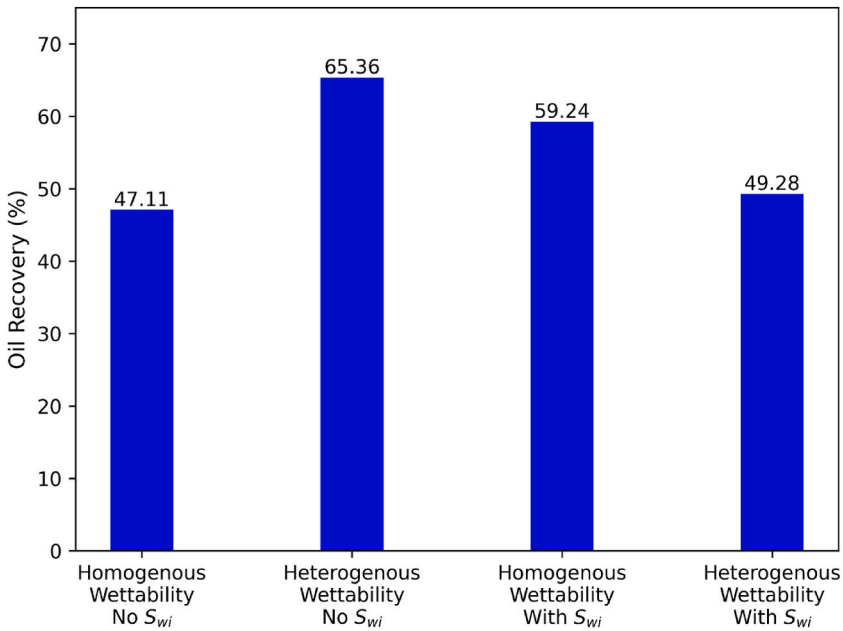

Fig. 18. Comparison of secondary HSWF performance in four different scenarios.

3.5.1. Secondary HSWF

Fig. 18 provides valuable insights into the performance of secondary HSWF in heterogeneous wettability conditions, particularly in the absence of S_{wi}. It is evident from the results that secondary HSWF leads to the most favorable oil recovery rate, achieving 65.36 % of OOIP. A compelling comparison emerges when assessing homogeneous and heterogeneous wettability scenarios in the absence of S_{wi}. In such conditions, heterogeneous wettability demonstrates a remarkable advantage, securing an 18.25 % higher oil recovery rate. This disparity can be attributed to the presence of water and neutral-wet regions within the designed pore structure. These regions provide favorable pathways for water to traverse and access a larger portion of the porous medium, leading to increased oil recovery.

However, the dynamics change when S_{wi} is introduced into the system. In this context, the continuous water phase within the pore structure facilitates the injection of water. Additionally, the presence of heterogeneous wettability in water-wet regions aids in displacing oil through the initially saturated water. Consequently, the oil recovery achieved by secondary HSWF in the presence of S_{wi} under heterogeneous wettability conditions is lower, amounting to 9.96 % of OOIP, compared to homogeneous wettability. These findings underscore the intricate interplay between wettability conditions and S_{wi} in influencing the effectiveness of secondary waterflooding techniques for oil recovery in heterogeneous reservoir systems.

3.5.2. Tertiary LSWF

LSWF behavior as a tertiary recovery method in homogeneous wettability conditions, in the absence of S_{wi}, demonstrates a remarkable capability to achieve substantial additional oil recovery, amounting to 35.83 % of OOIP. In contrast, when compared to heterogeneous wettability conditions, the incremental oil recovery is only 1.45 %. This suggests that in heterogeneous wettability scenarios, the effectiveness of LSWF in reducing contact angles and promoting a more water-wet environment is less pronounced than in homogeneous wettability conditions.

This disparity in effectiveness can be attributed to the variation in contact angles within different regions of the reservoir. In heterogeneous wettability scenarios, where oil fractions range from 80 to 100 % and 60–80 %, the contact angles for fully saturated LSW are 85 and 75°, respectively. In contrast, in homogeneous wettability scenarios, the contact angle for LSWF remains constant at 45° across all regions. As a result, in situations where S_{wi} is absent, the reduction in IFT from 0.02 N m^{-1} to 0.005 N.m^{-1}plays a significant role in enhancing oil recovery.

Conversely, in scenarios featuring S_{wi}, the distribution of oil and HSW prior to LSW injection, coupled with the presence of a continuous oil phase, particularly in heterogeneous scenarios, leads to greater additional oil recovery compared to homogeneous conditions. However, despite this increase in incremental recovery, the overall recovery remains lower in heterogeneous conditions than in homogeneous conditions. This underscores the profound impact of phase distribution on the efficacy of tertiary LSWF. Visual representations of the results of the tertiary LSWF can be found in Fig. 19.

3.5.3. Secondary LSWF

Fig. 20 reveals that in the absence of S_{wi}, the scenario with homogeneous wettability achieves the highest oil recovery among all four scenarios. In homogeneous wettability conditions, where all walls exhibit the same wettability, the LSW can efficiently sweep nearly all the oil in the geometry, leaving only residual oil in dead-end regions.

Conversely, in scenarios with S_{wi}, heterogeneous wettability demonstrates a more favorable response to Secondary LSWF. This is

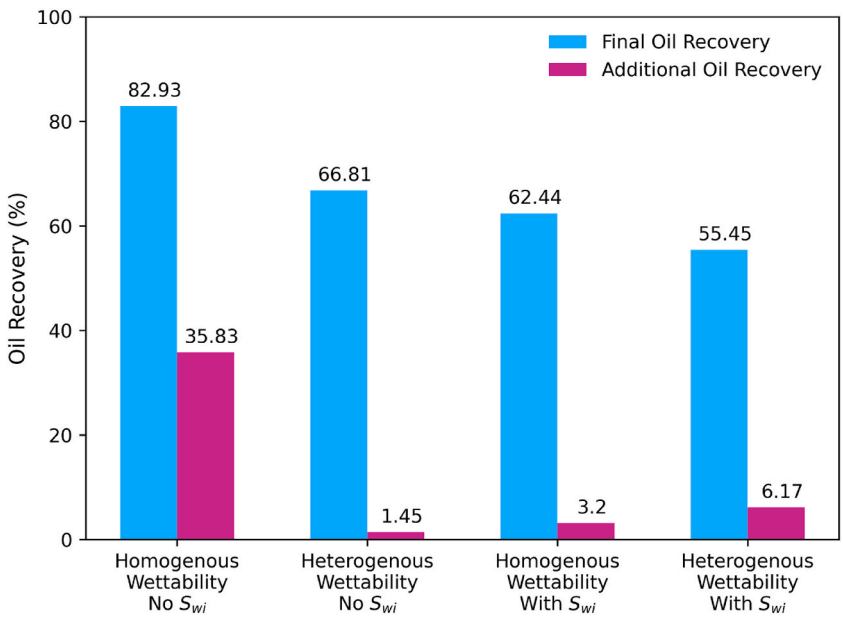

Fig. 19. Comparison of tertiary LSWF performance in four scenarios.

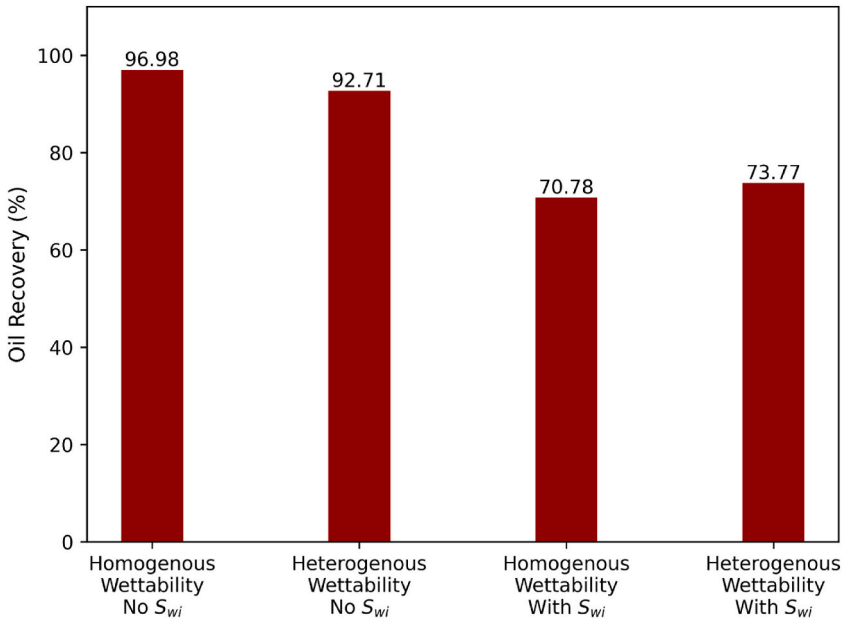

Fig. 20. Comparison of secondary LSWF performance in four different scenarios.

attributed to the S_{wi} aiding in faster breakthrough and the differences in wettability helping to maintain a more continuous oil phase, especially in comparison to homogeneous wettability. In homogeneous wettability scenarios, the LSWF front disperses the oil phase throughout the geometry before breaking through to the outlet, allowing some oil to remain within the geometry. In contrast, in heterogeneous wettability scenarios, the continuous oil phase is better preserved, resulting in a continuous push of the remaining oil toward the outlet. Consequently, this leads to higher oil recovery in heterogeneous wettability scenarios.

Figs. S–9 (Supplementary Material) demonstrates that among all the simulation cases, considering wettability distribution, the presence of S_{wi}, and various injection scenarios, secondary LSWF consistently exhibits the highest oil recovery. In general, the reported recovery values do not necessarily reflect the outcomes that might be observed on larger scales. This discrepancy can be attributed to factors such as the capillary number value, the favorable conditions assumed for the LSW phase, and the inherent nature of pore-scale simulation. Consequently, these reported values serve primarily as a macroscopic indicator to differentiate the outcomes of various implemented scenarios. Furthermore, despite our research focusing on LSWF at the pore scale, discrepancies persist between laboratory flooding experiments and field-scale pilot flooding. This disparity arises due to the complexity of the mechanisms involved and the influence of various factors, including operating conditions and the scale-dependence of effective parameters.

4. Conclusion

In this study, the effect of homogeneous and heterogeneous wettability conditions on LSWF performance in the presence and absence of S_{wi} is investigated. For this purpose, an OpenFOAM-based quasi-three-phase flow solver is used to capture wettability and IFT alteration determined by the varying fraction of LSW and HSW. To validate the solver, a pore-doublet geometry is designed for performing simulation and obtained results closely matched the experimental data. Additionally, a 2D heterogeneous geometry is designed for the main series of simulations. In total, we considered four scenarios for LSW injection, encompassing three types of injection: secondary HSWF, tertiary LSWF, and secondary LSWF.

Based on our simulations and findings, we draw the following conclusions.

- Overall, in all scenarios, secondary LSWF consistently achieves the highest oil recovery up to 96.98 %, aligning with several experimental findings. In heterogeneous wettability conditions, the efficiency of LSWF in tertiary mode may vary depending on the presence of S_{wi} and phase distribution.
- For secondary LSWF, homogeneous wettability conditions without S_{wi} yield the highest oil recovery (96.98 %) among all four scenarios. This behavior is attributed to the piston-like sweeping action that occurs due to consistent wall wettability in the geometry.
- In the case of secondary HSWF, heterogeneous wettability conditions without S_{wi} yield the highest oil recovery (65.36 %). This is attributed to the presence of water and neutral-wet conditions in the geometry, which outperform homogeneous conditions. However, in the presence of S_{wi}, homogeneous wettability conditions perform better than heterogeneous ones.
- The results of tertiary LSWF across the four scenarios reveal that a significant additional oil recovery up to 35.82 % is achieved in homogeneous wettability conditions in the absence of S_{wi}. Conversely, in heterogeneous wettability, characterized by multiple

wettability regions, wettability alteration alone does not contribute to additional oil recovery; only a minor oil recovery (1.45 %) is observed due to the reduction in IFT.

- When S_{wi} is considered, the distribution of oil and HSW before LSW injection results in a more favorable response to tertiary LSWF in heterogeneous wettability conditions. However, the total oil recovery remains lower than that of homogeneous wettability.
- In the presence of S_{wi}, secondary LSWF recovers less oil in homogeneous wettability conditions compared to heterogeneous ones by 2.99 %. This can be explained by the faster breakthrough in heterogeneous wettability facilitated by S_{wi} and the variations in wettability that maintain a continuous oil phase, subsequently pushing oil continuously towards the outlet.

Given that this study contributes to the literature by introducing a straightforward methodology for incorporating heterogeneous wettability distribution and initial water saturation during LSWF, there are several potential areas for future research that could enhance this foundation. The first potential area for future work is to obtain accurate wettability distribution. This can be achieved by utilizing QEMSCAN mineralogy assessments or by obtaining contact angle distribution from micro-CT images of core-flooding experiments. Another potential area for future work involves considering the chemical reactions and species involved in LSWF and their effect on contact angle variation. This could be achieved by coupling the current solver with a geochemical reaction solver like PHREEQC. Exploring larger-scale 3D digital models of actual formations and ensuring they satisfy the REV concept would enable investigation into larger-scale recovery mechanisms such as the gravity effect. Additionally, this would facilitate the examination of macroscopic parameters like relative permeability and fractional flow curves, and allow for the utilization of applicable upscaling approaches to compare outcomes with experimental studies. Investigating the effect of balancing capillary and viscous forces by altering the capillary number or pore-doublet dimensions in a pore-doublet focused study will provide valuable insights into the complex mechanisms of multiphase behavior during LSWF.

CRediT authorship contribution statement

Mahdi Malakoutikhah: Formal analysis, Methodology, Software, Writing – original draft. **Javad Siavashi:** Conceptualization, Formal analysis, Writing – review & editing. **Jalal Fahimpour:** Supervision, Writing – review & editing. **Mohammad Sharifi:** Conceptualization, Project administration, Resources, Supervision, Writing – review & editing.

Declaration of competing interest

The authors declare that they have no known competing financial interests or personal relationships that could have appeared to influence the work reported in this paper.

Appendix A. Supplementary data

Supplementary data to this article can be found online at https://doi.org/10.1016/j.heliyon.2024.e33303.

References

[1] M.H. Derkani, A.J. Fletcher, W. Abdallah, B. Sauerer, J. Anderson, Z.J. Zhang, Low salinity waterflooding in carbonate reservoirs: review of interfacial mechanisms, Colloids and Interfaces 2 (2018) 20, https://doi.org/10.3390/colloids2020020.
[2] F. Liu, M. Wang, Review of low salinity waterflooding mechanisms: wettability alteration and its impact on oil recovery, Fuel 267 (2020) 117112, https://doi.org/10.1016/j.fuel.2020.117112.
[3] H. Ding, S. Rahman, Experimental and theoretical study of wettability alteration during low salinity water flooding-an state of the art review, Colloids Surfaces A Physicochem Eng Asp 520 (2017) 622–639, https://doi.org/10.1016/j.colsurfa.2017.02.006.
[4] Y. Chen, Q. Xie, A. Sari, P.V. Brady, A. Saeedi, Oil/water/rock wettability: influencing factors and implications for low salinity water flooding in carbonate reservoirs, Fuel 215 (2018) 171–177, https://doi.org/10.1016/j.fuel.2017.10.031.
[5] A. Gandomkar, M.R. Rahimpour, Investigation of low-salinity waterflooding in secondary and tertiary enhanced oil recovery in limestone reservoirs, Energy Fuel. 29 (2015) 7781–7792, https://doi.org/10.1021/acs.energyfuels.5b01236.
[6] W. Song, A.R. Kovscek, Functionalization of micromodels with kaolinite for investigation of low salinity oil-recovery processes, Lab Chip 15 (2015) 3314–3325, https://doi.org/10.1039/C5LC00544B.
[7] A.B.D. Cassie, S. Baxter, Wettability of porous surfaces, Trans. Faraday Soc. 40 (1944) 546–551.
[8] M. Alizadeh, M. Fatemi, Mechanistic study of the effects of dynamic fluid/fluid and fluid/rock interactions during immiscible displacement of oil in porous media by low salinity water: direct numerical simulation, J. Mol. Liq. 322 (2021) 114544, https://doi.org/10.1016/j.molliq.2020.114544.
[9] T. Bultreys, L. Van Hoorebeke, V. Cnudde, Multi-scale, micro-computed tomography-based pore network models to simulate drainage in heterogeneous rocks, Adv. Water Resour. 78 (2015) 36–49, https://doi.org/10.1016/j.advwatres.2015.02.003.
[10] Z. Qin, S. Esmaeilzadeh, A. Riaz, H.A. Tchelepi, Two-phase multiscale numerical framework for modeling thin films on curved solid surfaces in porous media, J. Comput. Phys. 413 (2020) 109464, https://doi.org/10.1016/j.jcp.2020.109464.
[11] P. Daripa, S. Dutta, Modeling and simulation of surfactant–polymer flooding using a new hybrid method, J. Comput. Phys. 335 (2017) 249–282, https://doi.org/10.1016/j.jcp.2017.01.038.
[12] M. Mahdaviara, M.J. Shojaei, J. Siavashi, M. Sharifi, M.J. Blunt, Deep learning for multiphase segmentation of X-ray images of gas diffusion layers, Fuel 345 (2023) 128180, https://doi.org/10.1016/j.fuel.2023.128180.
[13] J. Siavashi, A. Najafi, A. Moslemizadeh, M. Sharifi, E. Kowsari, S. Zendehboudi, Design and synthesis of a new ionic liquid surfactant for petroleum industry, J. Mol. Liq. 367 (2022) 120047, https://doi.org/10.1016/j.molliq.2022.120047.
[14] S. Aldousary, A.R. Kovscek, The diffusion of water through oil contributes to spontaneous emulsification during low salinity waterflooding, J. Pet. Sci. Eng. 179 (2019) 606–614.

[15] R. Aziz, V. Niasar, H. Erfani, P.J. Martínez-Ferrer, Impact of pore morphology on two-phase flow dynamics under wettability alteration, Fuel 268 (2020) 117315, https://doi.org/10.1016/j.fuel.2020.117315.
[16] A. Najafi, J. Siavashi, M. Ebadi, D. Orlov, M. Sharifi, J. Fahimpour, et al., Using computational fluid dynamics to compute the pore-scale CO2-brine relative permeability, Fuel 341 (2023) 127715, https://doi.org/10.1016/j.fuel.2023.127715.
[17] T. Ramstad, C.F. Berg, K. Thompson, Pore-scale simulations of single- and two-phase flow in porous media: approaches and applications, Transport Porous Media 130 (2019) 77–104, https://doi.org/10.1007/s11242-019-01289-9.
[18] J. Siavashi, A. Najafi, M. Ebadi, M. Sharifi, A CNN-based approach for upscaling multiphase flow in digital sandstones, Fuel 308 (2022) 122047, https://doi.org/10.1016/j.fuel.2021.122047.
[19] A. Rabbani, P. Mostaghimi, R.T. Armstrong, Pore network extraction using geometrical domain decomposition, Adv. Water Resour. 123 (2019) 70–83, https://doi.org/10.1016/j.advwatres.2018.11.003.
[20] P. Rostami, M.F. Mehraban, M. Sharifi, M. Dejam, S. Ayatollahi, Effect of water salinity on oil/brine interfacial behaviour during low salinity waterflooding: a mechanistic study, Petroleum 5 (2019) 367–374, https://doi.org/10.1016/j.petlm.2019.03.005.
[21] A. Katende, F. Sagala, A critical review of low salinity water flooding: mechanism, laboratory and field application, J. Mol. Liq. 278 (2019) 627–649, https://doi.org/10.1016/j.molliq.2019.01.037.
[22] M. Sohrabi, P. Mahzari, S.A. Farzaneh, J.R. Mills, P. Tsolis, S. Ireland, Novel insights into mechanisms of oil recovery by use of low-salinity-water injection, SPE J. 22 (2017) 407–416, https://doi.org/10.2118/172778-PA.
[23] M.J. Barnaji, P. Pourafshary, M.R. Rasaie, Visual investigation of the effects of clay minerals on enhancement of oil recovery by low salinity water flooding, Fuel 184 (2016) 826–835, https://doi.org/10.1016/j.fuel.2016.07.076.
[24] M. Ghasemi, A. Shafiei, J. Foroozesh, A systematic and critical review of application of molecular dynamics simulation in low salinity water injection, Adv. Colloid Interface Sci. 300 (2022) 102594, https://doi.org/10.1016/j.cis.2021.102594.
[25] J. Batias, G. Hamon, B. Lalanne, C. Romero, Field and laboratory observations of Remaining oil saturations in a light oil reservoir flooded by a low salinity aquifer. Pap. SCA2009-01 Present. 23rd Int. Symp. Soc. Core Anal. Noordwijk Aan Zee, 2009, pp. 27–30. Netherlands.
[26] H. Mahani, T.G. Sorop, D. Ligthelm, A.D. Brooks, P. Vledder, F. Mozahem, et al., Analysis of field responses to low-salinity waterflooding in secondary and tertiary mode in Syria. SPE Eur Annu Conf Exhib, 2011, https://doi.org/10.2118/142960-MS. SPE-142960-MS.
[27] K. Skrettingland, T. Holt, M.T.T. Tweheyo, I. Skjevrak, Snorre low-salinity-water injection—coreflooding experiments and single-well field pilot, SPE Reservoir Eval. Eng. 14 (2011) 182–192, https://doi.org/10.2118/129877-PA.
[28] G. Tang, N.R. Morrow, Oil recovery by waterflooding and imbibition-invading brine cation valency and salinity, Pap SCA9911 (1999).
[29] W. Song, A.R. Kovscek, Direct visualization of pore-scale fines migration and formation damage during low-salinity waterflooding, J. Nat. Gas Sci. Eng. 34 (2016) 1276–1283.
[30] M. Yu, A. Zeinijahromi, P. Bedrikovetsky, L. Genolet, A. Behr, P. Kowollik, et al., Effects of fines migration on oil displacement by low-salinity water, J. Pet. Sci. Eng. 175 (2019) 665–680.
[31] M. Cissokho, H. Bertin, S. Boussour, P. Cordier, G. Hamon, Low salinity oil recovery on clayey sandstone: experimental study, Petrophysics-The SPWLA J Form Eval Reserv Descr 51 (2010).
[32] S. Berg, A.W. Cense, E. Jansen, K. Bakker, Direct experimental evidence of wettability modification by low salinity, Petrophysics-The SPWLA J Form Eval Reserv Descr 51 (2010).
[33] Y. Zhang, X. Xie, N.R. Morrow, Waterflood performance by injection of brine with different salinity for reservoir cores. SPE Annu, Tech. Conf. Exhib., OnePetro, 2007.
[34] A. Lager, K.J. Webb, C.J.J. Black, M. Singleton, K.S. Sorbie, Low salinity oil recovery-an experimental investigation1, Petrophysics-The SPWLA J Form Eval Reserv Descr 49 (2008).
[35] T. Austad, A. RezaeiDoust, T. Puntervold, Chemical mechanism of low salinity water flooding in sandstone reservoirs. SPE Improved Oil Recovery Symposium, Society of Petroleum Engineers. Pap SPE, Tulsa, Oklahoma, 2010 129767.
[36] P. Vledder, J.C. Fonseca, T. Wells, I. Gonzalez, D. Ligthelm, Low salinity water flooding: proof of wettability alteration on a field wide scale, in: SPE Improved Oil Recovery Conference, 2010. https://doi.org/10.2118/129564-MS. SPE-129564-MS.
[37] W.O. Winsauer, W.M. McCardell, Ionic double-layer conductivity in reservoir rock, J. Petrol. Technol. 5 (1953) 129–134.
[38] D.J. Ligthelm, J. Gronsveld, J.P. Hofman, N.J. Brussee, F. Marcelis, H.A. Van der Linde, Novel Waterflooding Strategy by Manipulation of Injection Brine Composition, Eur. Conf. Exhib., OnePetro, 2009.
[39] R.A. Nasralla, H.A. Nasr-El-Din, Double-layer expansion: is it a primary mechanism of improved oil recovery by low-salinity waterflooding? SPE Reservoir Eval. Eng. 17 (2014) 49–59.
[40] M. Mehana, M.M. Fahes, Investigation of double layer expansion in low-salinity waterflooding: molecular simulation study, in: SPE West. Reg. Meet, OnePetro, 2018.
[41] J.S. Buckley, K. Takamura, N.R. Morrow, SPE reservoir engineering, Influ Electr Surf Charg Wetting Prop Crude Oils 4 (1989) 332–340.
[42] J. Chen, G.J. Hirasaki, M. Flaum, NMR wettability indices: effect of OBM on wettability and NMR responses, J. Pet. Sci. Eng. 52 (2006) 161–171.
[43] P. Zhang, M.T. Tweheyo, T. Austad, Wettability alteration and improved oil recovery by spontaneous imbibition of seawater into chalk: impact of the potential determining ions Ca2+, Mg2+, and SO42, Colloids Surfaces A Physicochem Eng Asp 301 (2007) 199–208.
[44] M. Mohammed, T. Babadagli, Wettability alteration: a comprehensive review of materials/methods and testing the selected ones on heavy-oil containing oil-wet systems, Adv. Colloid Interface Sci. 220 (2015) 54–77.
[45] B.D. Saikia, J. Mahadevan, D.N. Rao, Exploring mechanisms for wettability alteration in low-salinity waterfloods in carbonate rocks, J. Pet. Sci. Eng. 164 (2018) 595–602.
[46] J. Buckley, Low Salinity Waterflooding-An Overview of Likely Mechanisms, 2009 on-line presentation.
[47] A.A. Yousef, S.C. Ayirala, A novel water ionic composition optimization technology for SmartWater flooding application in carbonate reservoirs, in: SPE Improv. Oil Recover. Symp., OnePetro, 2014.
[48] C. Callegaro, M. Bartosek, F. Masserano, M. Nobili, V.P. Parracello, C.S. Pizzinelli, et al., Opportunity of Enhanced Oil Recovery Low Salinity Water Injection: from Experimental Work to Simulation Study up to Field Proposal, EAGE Annu. Conf. Exhib. Inc. SPE Eur., OnePetro, 2013.
[49] M. Rotondi, C. Callegaro, F. Masserano, M. Bartosek, Low salinity water injection: eni's experience, in: Abu Dhabi International Petroleum Exhibition and Conference, 2014. D041S074R005, https://doi.org/10.2118/171794-MS.
[50] S.B. Fredriksen, A.U. Rognmo, M.A. Fernø, Pore-scale mechanisms during low salinity waterflooding: oil mobilization by diffusion and osmosis, J. Pet. Sci. Eng. 163 (2018) 650–660.
[51] K. Sandengen, A. Kristoffersen, K. Melhuus, L.O. Jøsang, Osmosis as mechanism for low-salinity enhanced oil recovery, SPE J. 21 (2016) 1227–1235.
[52] S.B. Fredriksen, A.U. Rognmo, K. Sandengen, M.A. Fernø, Wettability effects on osmosis as an oil-mobilization mechanism during low-salinity waterflooding, Petrophysics 58 (2017) 28–35.
[53] E.N. Pollen, C.F. Berg, Experimental investigation of osmosis as a mechanism for low-salinity EOR, in: Abu Dhabi International Petroleum Exhibition and Conference, 2018. D022S139R001, https://doi.org/10.2118/192753-MS.
[54] T. Austad, Water-based EOR in carbonates and sandstones: new chemical understanding of the EOR potential using "smart water.". Enhanc. Oil Recover. F. Case Stud., Elsevier, 2013, pp. 301–335.
[55] A. Kakati, J.S. Sangwai, Effect of monovalent and divalent salts on the interfacial tension of pure hydrocarbon-brine systems relevant for low salinity water flooding, J. Pet. Sci. Eng. 157 (2017) 1106–1114.
[56] T. Kar, H. Cho, A. Firoozabadi, Assessment of low salinity waterflooding in carbonate cores: interfacial viscoelasticity and tuning process efficiency by use of non-ionic surfactant, J. Colloid Interface Sci. 607 (2022) 125–133, https://doi.org/10.1016/j.jcis.2021.08.028.

[57] R. Aziz, V. Joekar-Niasar, P.J. Martínez-Ferrer, O.E. Godinez-Brizuela, C. Theodoropoulos, H. Mahani, Novel insights into pore-scale dynamics of wettability alteration during low salinity waterflooding, Sci. Rep. 9 (2019) 9257, https://doi.org/10.1038/s41598-019-45434-2.
[58] W.-B. Bartels, H. Mahani, S. Berg, S.M. Hassanizadeh, Literature review of low salinity waterflooding from a length and time scale perspective, Fuel 236 (2019) 338–353.
[59] H. Mahani, S. Berg, D. Ilic, W.-B.-B. Bartels, V. Joekar-Niasar, Kinetics of low-salinity-flooding effect, SPE J. 20 (2015) 8–20.
[60] G.Q. Tang, N.R. Morrow, Salinity, temperature, oil composition, and oil recovery by waterflooding, SPE Reservoir Eng. 12 (1997) 269–276.
[61] T. Bultreys, W. De Boever, V. Cnudde, Imaging and image-based fluid transport modeling at the pore scale in geological materials: a practical introduction to the current state-of-the-art, Earth Sci. Rev. 155 (2016) 93–128, https://doi.org/10.1016/j.earscirev.2016.02.001.
[62] E.V. Lavrukhin, K.M. Gerke, K.A. Romanenko, K.N. Abrosimov, M.V. Karsanina, Assessing the fidelity of neural network-based segmentation of soil XCT images based on pore-scale modelling of saturated flow properties, Soil Tillage Res. 209 (2021) 104942, https://doi.org/10.1016/j.still.2021.104942.
[63] A.M. Selem, N. Agenet, Y. Gao, A.Q. Raeini, M.J. Blunt, B. Bijeljic, Pore-scale imaging and analysis of low salinity waterflooding in a heterogeneous carbonate rock at reservoir conditions, Sci. Rep. 11 (2021) 15063.
[64] J. Goral, M. Andrew, T. Olson, M. Deo, Correlative core- to pore-scale imaging of shales, Mar. Petrol. Geol. 111 (2020) 886–904, https://doi.org/10.1016/j.marpetgeo.2019.08.009.
[65] Y. Da Wang, M.J. Blunt, R.T. Armstrong, P. Mostaghimi, Deep learning in pore scale imaging and modeling, Earth Sci. Rev. 215 (2021) 103555.
[66] C.F. Berg, O. Lopez, H. Berland, Industrial applications of digital rock technology, J. Pet. Sci. Eng. 157 (2017) 131–147, https://doi.org/10.1016/j.petrol.2017.06.074.
[67] B. Zhao, C.W. MacMinn, B.K. Primkulov, Y. Chen, A.J. Valocchi, J. Zhao, et al., Comprehensive comparison of pore-scale models for multiphase flow in porous media, Proc. Natl. Acad. Sci. USA 116 (2019) 13799–13806, https://doi.org/10.1073/pnas.1901619116.
[68] Y. Yang, K. Wang, L. Zhang, H. Sun, K. Zhang, J. Ma, Pore-scale simulation of shale oil flow based on pore network model, Fuel 251 (2019) 683–692, https://doi.org/10.1016/j.fuel.2019.03.083.
[69] A.Q. Raeini, M.J. Blunt, B. Bijeljic, Direct simulations of two-phase flow on micro-CT images of porous media and upscaling of pore-scale forces, Adv. Water Resour. 74 (2014) 116–126, https://doi.org/10.1016/j.advwatres.2014.08.012.
[70] D. Orlov, M. Ebadi, E. Muravleva, D. Volkhonskiy, A. Erofeev, E. Savenkov, et al., Different methods of permeability calculation in digital twins of tight sandstones, J. Nat. Gas Sci. Eng. 87 (2021) 103750, https://doi.org/10.1016/j.jngse.2020.103750.
[71] M.J. Blunt, B. Bijeljic, H. Dong, O. Gharbi, S. Iglauer, P. Mostaghimi, et al., Pore-scale imaging and modelling, Adv. Water Resour. 51 (2013) 197–216, https://doi.org/10.1016/j.advwatres.2012.03.003.
[72] G. Zhu, J. Yao, A. Li, H. Sun, L. Zhang, Pore-scale investigation of carbon dioxide-enhanced oil recovery, Energy Fuel. 31 (2017) 5324–5332, https://doi.org/10.1021/acs.energyfuels.7b00058.
[73] X. Yang, T.D. Scheibe, M.C. Richmond, W.A. Perkins, S.J. Vogt, S.L. Codd, et al., Direct numerical simulation of pore-scale flow in a bead pack: comparison with magnetic resonance imaging observations, Adv. Water Resour. 54 (2013) 228–241, https://doi.org/10.1016/j.advwatres.2013.01.009.
[74] M.E. Kutay, A.H. Aydilek, E. Masad, Laboratory validation of lattice Boltzmann method for modeling pore-scale flow in granular materials, Comput. Geotech. 33 (2006) 381–395, https://doi.org/10.1016/j.compgeo.2006.08.002.
[75] H. Mo, Y. Yong, K. Yu, W. Chen, J. Dai, C. Yang, An integrated Lattice-Boltzmann model of immiscible two-phase flow and bulk mass transfer with Marangoni effect, J. Comput. Phys. 481 (2023) 112037, https://doi.org/10.1016/j.jcp.2023.112037.
[76] N.J. Taylor, CFD Validation: what Is it and How Do We Effect it? AIAA Aviat. 2022 Forum, American Institute of Aeronautics and Astronautics, Reston, Virginia, 2022, https://doi.org/10.2514/6.2022-3768.
[77] Y. Zaretskiy, S. Geiger, K. Sorbie, Direct numerical simulation of pore-scale reactive transport: applications to wettability alteration during two-phase flow, Int. J. Oil Gas Coal Technol. 5 (2012) 142, https://doi.org/10.1504/IJOGCT.2012.046318.
[78] J. Maes, S. Geiger, Direct pore-scale reactive transport modelling of dynamic wettability changes induced by surface complexation, Adv. Water Resour. 111 (2018) 6–19, https://doi.org/10.1016/j.advwatres.2017.10.032.
[79] M.O. Abu-Al-Saud, S. Esmaeilzadeh, A. Riaz, H.A. Tchelepi, Pore-scale study of water salinity effect on thin-film stability for a moving oil droplet, J. Colloid Interface Sci. 569 (2020) 366–377, https://doi.org/10.1016/j.jcis.2020.02.044.
[80] S. An, Y. Zhan, H. Mahani, V. Niasar, Kinetics of wettability alteration and droplet detachment from a solid surface by low-salinity: a lattice-Boltzmann method, Fuel 329 (2022) 125294, https://doi.org/10.1016/j.fuel.2022.125294.
[81] A. Pourakaberian, H. Mahani, V. Niasar, Dynamics of electrostatic interaction and electrodiffusion in a charged thin film with nanoscale physicochemical heterogeneity: implications for low-salinity waterflooding, Colloids Surfaces A Physicochem Eng Asp 650 (2022) 129514, https://doi.org/10.1016/j.colsurfa.2022.129514.
[82] T. Akai, A.M. Alhammadi, M.J. Blunt, B. Bijeljic, Mechanisms of microscopic displacement during enhanced oil recovery in mixed-wet rocks revealed using direct numerical simulation, Transport Porous Media 130 (2019) 731–749, https://doi.org/10.1007/s11242-019-01336-5.
[83] M. Alizadeh, M. Fatemi, Pore-doublet computational fluid dynamic simulation of the effects of dynamic contact angle and interfacial tension alterations on the displacement mechanisms of oil by low salinity water, Int. J. Multiphas. Flow 143 (2021) 103771, https://doi.org/10.1016/j.ijmultiphaseflow.2021.103771.
[84] M. Alizadeh, M. Fatemi, M. Mousavi, Direct numerical simulation of the effects of fluid/fluid and fluid/rock interactions on the oil displacement by low salinity and high salinity water: pore-scale occupancy and displacement mechanisms, J. Pet. Sci. Eng. 196 (2021) 107765, https://doi.org/10.1016/j.petrol.2020.107765.
[85] A. Namaee-Ghasemi, S. Ayatollahi, H. Mahani, Pore-scale simulation of the interplay between wettability, capillary number, and salt dispersion on the efficiency of oil mobilization by low-salinity waterflooding, SPE J. 26 (2021) 4000–4021, https://doi.org/10.2118/206728-PA.
[86] I. Chatzis, F.A. Dullien, Dynamic immiscible displacement mechanisms in pore doublets: theory versus experiment, J. Colloid Interface Sci. 91 (1983) 199–222, https://doi.org/10.1016/0021-9797(83)90326-0.